Using multi-objective sparrow search algorithm to establish active distribution network dynamic reconfiguration integrated optimization

Abstract

This study contributes to establish the dynamic reconfiguration integrated optimization model of active distribution network (ADN) and proposes a novel solving approach based on multi-objective sparrow search algorithm. Distributed generation and time-varying load have an important impact on promoting sustainable development and reducing energy loss. Therefore, this study aims to investigate the ADN integrated optimization problem in consideration of distributed generation and time-varying load to improve the ADN power quality, economic and energy benefits. First, a multi-objective sparrow search algorithm is proposed aiming at the multi-objective, multi-constraint, non-linear and high-dimensional ADN integrated optimization problem, and the superiority of the proposed algorithm is verified. Second, the mathematical model of ADN integrated optimization is constructed. Finally, multi-scenario test is conducted in the classic test system to verify the effectiveness of proposed method, and the compromise solution is determined through the technique for order of preference by similarity to ideal solution (TOPSIS). The result shows that the proposed method effectively reduces the power loss and node voltage deviation by 75.76% and 70.06%. Accordingly, this study is significance for improving the operational stability of ADN, increasing the penetration rate of renewable energy and promoting economic production.

Keywords: active distribution network; dynamic reconfiguration; integrated optimization; multi-objective sparrow search algorithm; renewable energy

Definition of acronyms and variables

Acronyms		**Variables**	
ADN	Active distribution network	C_a	Operating loss coefficient ($/kW)
Archive	External archive size	C_b	Unit action cost of the connection switch ($/time)
CD	Critical difference		
DG	Distributed generation	C_e	Electricity price ($/kWh)
HV	Hypervolume	C_r	Total operating cost ($)
I	Current	Dis	Euclidean distance
IEEE 33	Institute of electrical and electronic engineering designed standard test system with 33 nodes	f	Objective function
		G, θ, B	Real part, impedance angle and imaginary part of the admittance
IGD	Inverted generational distance	N	Population size
MOGWO	Multi-objective gray wolf optimization	N_b	Number of branches
		N_m	Node number
MOMVO	Multi-objective multi-verse optimization	N_n	Number of nodes
		N_S	Number of connecting switch actions
MOPSO	Multi-objective particle swarm optimization	$\{N_{SC}\}^{node}$	{Shunt capacitor number}$^{\text{node number}}$
		N_t	Number of compensation equipment
MOSSA	Multi-objective sparrow search algorithm	P	Active power (kW)
		P_{DG}	DG active power output (kW)
NIS	Negative ideal solutions	Q_{DG}	DG reactive power output (kVar)
NSGA-II	Non-dominated sorting genetic algorithm with elite strategy	P_{load}	Residential load active power (kW)
		Q_{load}	Living load reactive power(kVar)
NSMFO	Non-dominated sorting moth flame optimization	P_{loss}	Active power loss (kW)
		Q_{loss}	reactive power loss (kVar)
PIS	Positive ideal solutions	Q	Reactive power (KVar)
PV	Photovoltaic	$\{Q_{SVC}\}^{node}$	{SVC reactive power output}$^{\text{node number}}$
SC	Shunt capacitor	R_1, R_2	Early warning value and safety value
SP	Spacing	t	Current number of iterations
SSA	Sparrow search algorithm	T_{max}	Maximum number of iterations
SVC	Static var compensator	U	Voltage (kV)
TOPSIS	Technique for order preference by similarity to ideal solution	W	Population scale factor
		X^{SC}	SC access group number
WT	Wind turbine	X^{SVC}	SVC reactive power output (kVar)
ZDT	Zero-ductility transition	X^{Swich}	Disconnection switch number

Using multi-objective sparrow search algorithm to establish active distribution network dynamic reconfiguration integrated optimization

1. Introduction

The penetration of clean and sustainable energy sources is increasing in modern power systems due to the continuous growth of global energy demand (Singh et al., 2020). Clean energy sources will gradually replace fossil energy sources in the future (Acharya et al, 2021; Coelho and Mariani, 2007). Fossil energy production and consumption has led to a range of problems (Chen and Tang, 2022; Coelho and Mariani, 2006). The consumption of fossil energy destroys the environment, so there is an urgent need for large amounts of clean energy to replace fossil energy (Liu et al., 2021; Coelho et al.,2014). Clean energy is a renewable energy source that has an important impact on sustainable development and environmental improvement (Sun et al., 2021; Tseng et al., 2021; Mellal and Williams., 2020). However, distributed energy sources have an impact on the power system (Li et al., 2021; Coelho and Mariani., 2009).

Especially, in modern power system, the distribution network injects a high-density distributed generation (DG), which changes the original distribution network structure (Kiani et al., 2021). The output of DG has strong randomness and intermittency, which increases the complexity and uncertainty of the system. It will cause great changes in node voltage, power flow direction, network loss and branch power, and severely impact the economic and safe operation of the system (Xu et al., 2021). Nick et al. (2014) argues that technologies such as network reconfiguration and reactive power optimization can effectively optimize the distribution network operation. Active distribution network (ADN) is a distribution network with DGs inside, flexible topology adjustment and active control capability.

Network reconfiguration changes the connection switch state to obtain the optimal power flow distribution under a set of constraints, so as to balance the load, improve the equipment utilization, increase the voltage stability and minimize the network loss (Cheng and Li, 2019). However, reactive power optimization is a complex multi-dimensional problem. Its control variables include static var compensator (SVC) compensation capacity, shunt capacitor (SC) input group number and so on (Ma et al., 2021). In system, reactive power optimization can reduce network loss, improve voltage distribution, reduce power generation cost and improve energy utilization (Chen et al., 2021). In sum, this study is necessary to find a model that can consider network reconfiguration and reactive power collaborative optimization, so as to maximize the comprehensive benefits of electric energy in the production and distribution process.

In the current studies of distribution network reconfiguration, it is divided into static reconfiguration and dynamic reconfiguration according to different time periods. Static reconfiguration is to find the optimal topology for a certain period of time when the load power and the output of DG are constant (Azad-Farsani et al., 2021). It is the optimization of ADN based on fixed load and constant generation conditions. Yet, ADN must be dynamically reconfigured in consideration of the time-varying resident load and fluctuation of DG output, as well as other random factors. Dynamic reconfigured considers the operating conditions which include random output of DG and time-varying load in a continuous period of time (Ji

et al., 2021). ADN has a vast area and complex network topology. Therefore, the dynamic reconfiguration and reactive power collaborative optimization of ADN is a multi-objective, multi-dimensional, multi-variable and multi-constraint problem.

Many literatures only convert the multi-objective optimization problem into single-objective optimization problem or conducts single-objective optimization to solve the problem. Only a few literatures regard it as a practical multi-objective problem. The major methods to deal with multi-objective problems include weighting method (Olamaei et al., 2008), fuzzy set theory (Kefayat et al., 2015), penalty function method (Oh et al., 2020), Pareto optimal frontier (Raposo et al., 2020) and non-dominated sorting (Duan et al., 2015). The weighting method has fast solving speed and transforms multi-objective into single-objective. However, the weights are set in advance. The objective functions in actual problems may have complex coupling relationships, so the actual optimal value cannot be obtained (Ramaswamy et al., 2015). The penalty function method restricts the target space by penalizing infeasible solutions, but requires a higher penalty factor (Coello Coello, 2002). The Pareto optimal frontier is a solution set, which cannot reflect the trade-off between multiple goals. Adopting non-dominated sorting may destroy the spatial distribution and diversity of solution.

Aiming at the gaps in the above-mentioned literatures, this study considers distributed generation, time-varying load and real-time electricity prices in the ADN integrated optimization problem, as well as the contradictory relationship between power quality, economic efficiency and energy loss. Meanwhile, a multi-objective sparrow search algorithm is proposed based on the characteristics of ADN integrated optimization problem, such as multi-objective, multi-constraint, non-linear and high-dimensional. Finally, multiple scenarios in the IEEE 33 system are used to verify the effectiveness of the proposed method. Additionally, the contributions of this study are as follows.

- A dynamic reconfiguration integrated optimization model of ADN considering load time variation, real-time electricity price and fluctuation of DG output is constructed.
- A novel multi-objective sparrow search algorithm (MOSSA) with better performance is proposed to solve the multi-objective, multi-constraint, non-linear and high-dimensional integrated optimization problem of ADN. MOSSA has better convergence speed, stronger search capability and higher quality solutions compared with current excellent multi-objective algorithms.
- Adopting MOSSA to solve the ADN problem, and the solution obtained by the proposed method has been proven to outperform the results obtained by the existing algorithms through multiple scenarios compared in the IEEE 33 system.
- The proposed MOSSA effectively reduces ADN energy losses, improves power quality and economic efficiency, and further increases the efficiency and penetration of renewable energy.

This study is organized as follows: Chapter 2 surveys the literature on network reconfiguration and reactive power optimization. Chapter 3 introduces the ADN dynamic reconfiguration integrated optimization model and its optimization method. Chapter 4 verifies the effectiveness of the proposed model in different scenarios of IEEE 33 system.

Chapter 5 summarizes the concluding remarks, analyzes the shortcomings of this study and proposes future research prospects.

2. Literature review

Integrated optimization of active distribution network (ADN) has received significant attention due to the rapid growth of distributed energy sources in power system (Qian and Sui, 2021). Prior studies have proposed some ADN optimization tools, such as network reconfiguration and reactive power optimization. Network reconfiguration changes the switch connection state to optimize ADN operation. Reactive power optimization is achieved by reactive power compensation device output to compensate the system reactive power.

Methods that use network reconstruction to achieve ADN optimization include particle swarm optimization (Mukhopadhyay and Das, 2020), genetic algorithm (Gupta et al., 2014), simulated annealing immunity algorithm (Chen et al., 2011), gray wolf algorithm (Nguyen et al., 2014), ant colony algorithm (Su et al., 2005), stochastic fractal search algorithm (Tran et al., 2020). Since the metaheuristic algorithms generally converge slowly, Nguyen et al. (2019) proposes an improved cuckoo search algorithm to solve the ADN reconstruction problem, which is able to find the global optimal solution with fewer iterations, but only considers the network loss ignoring renewable energy generation. Aiming to increase the renewable energy penetration, Pathan et al. (2020) uses an improved binary genetic algorithm based on the minimization of system operation interruption time and energy not supplied considering renewable energy sources and energy storage, which sets weights in advance according to individual preferences and transforms multiple objectives into a single objective, but there may be contradictory relationships between multiple objectives that can lead to not obtaining the actual optimal solution. Considering the contradictory relationship between objectives, Niknam et al. (2012) uses a multi-objective modified honey bee mating optimization algorithm for multi-objective optimization to find the Pareto optimal solution set and then select the optimal compromise solution using fuzzy clustering method, but only static reconstruction is performed.

In addition, ADN must be dynamically reconfigured due to load time-variability, increase in DG and other stochastic factors (Kovacki et al., 2018; Sheidaei et al., 2021; Sun et al., 2021). Jafari et al. (2020) proposes a new hybrid algorithm that combines the trading market algorithm and the wild goat algorithm for parallel operations to perform dynamic reconstruction of ADN, which improves the computational speed but ignores DG. Zidan et al. (2013) proposes a method for determining the annual reconfiguration that considers the variable load curve and stochastic generation of DG, which is optimized using a genetic algorithm, but only considers energy loss minimization ignoring the operating costs. Aiming to minimize the operating cost and energy loss, Azizivahed et al. (2018) considers the real-time tariff and the time-varying load to establish a dynamic reconfiguration model with the objectives of network loss, operating cost and energy consumption, and also proposes a hybrid algorithm to optimize this model. However, only network reconfiguration is performed, and there is a huge upside in ADN operational performance.

Reactive power optimization techniques are also widely used in ADN optimization. For

instance, Medani et al. (2018) uses the whale optimization algorithm to optimize the reactive power scheduling and find the optimal vector of control variables to achieve power loss reduction, but only considering the power loss. Aiming at multi-objective reactive power optimization, Medani et al. (2012) uses a simulated fisherman fishing optimization algorithm and proposes a reference area-based approach to improve the search speed. However, it only performs static optimization and does not perform dynamic optimization. Mahdad (2019) uses the fractal search algorithm for reactive power optimization resource scheduling, but ignores the effect of DG on the system and the optimization algorithm can be further improved. To further improve the performance of intelligent optimization algorithms, a variety of intelligent algorithm improvement methods are widely used to deal with more complex optimization problems (Gao et al., 2021; Tseng et al., 2021). Aiming at the problem of low accuracy of traditional particle swarm optimization (PSO), Zou (2021) proposes fuzzy particle swarm optimization algorithm based on PSO to establish static and dynamic mathematical models of the system for achieving reactive power optimization. However, the model only considers the network loss minimization, which cannot meet the practical requirements. To meet the practical needs, Wang et al. (2011) proposes a comprehensive and practical multi-objective reactive power optimization model, then adopts the fuzzy adaptive particle swarm algorithm optimization model, and finally uses fuzzy set theory to solve the multi-objective problem. However, this method converts multiple objectives into a single objective, but there may be contradictory relationships among the objective functions, so the actual optimal solution cannot be obtained.

Previous literature lacks research on ADN integrated optimization, which usually uses only one optimization tool, such as network reconfiguration or reactive power optimization. Only a few studies use multiple tools for ADN optimization. ADN integrated optimization using multiple techniques can maximize the ADN operational performance. For instance, Tolabi et al. (2020) proposes a new thief and police algorithm to perform network reconfiguration and optimize the configuration of DG and capacitors, but it lacks dynamic analysis. Raut et al. (2019) proposes a novel improved elite-Jaya algorithm to solve the simultaneous network reconfiguration and DG assignment problems, which converts the multi-objective into a single-objective optimization, ignoring the conflicting relationships between the objectives. Srinivasan et al. (2021) proposes an autonomous group particle swarm optimization algorithm for active distribution network optimization, which first performs reactive power compensation and then network reconfiguration, but lacks dynamic analysis and without considering the impact of DG and dynamic loads on the system.

In sum, previous studies lack to address the conflicting relationships between energy, power quality and economic efficiency. In addition, literature lacks tackling the impact of renewable energy generation and dynamic loads on modern power system and the use of multiple tools combined for ADN optimization. Therefore, this study constructs integrated optimization model of ADN considering DG, dynamic load and electricity price. Meanwhile, the dynamic reconstruction and reactive power optimization techniques are combined to optimize ADN, and MOSSA is proposed to solve the contradictory relationship between

power quality, economic efficiency and energy saving, which effectively reduces energy loss, promotes sustainable energy development and reduces economic cost.

3. Model description

This study considers three aspects: economic benefit, energy loss and power quality. Minimizing the economic cost, active power loss and node voltage deviation of ADN is the goal. Considering the fluctuation of DG output, real-time electricity price and time-varying load, a dynamic reconfiguration and reactive power collaborative optimization model of ADN is established.

3.1. Decision variables

The switch action state, static var compensator (SVC) compensation capacity and shunt capacitor (SC) access group number are selected as decision variables to obtain the optimal network topology and the output of reactive power compensation equipment in each period of ADN.

$$\boldsymbol{X} = \left[X_1^{\text{Swich}}, \ldots, X_a^{\text{Swich}}, X_1^{\text{SVC}}, \ldots, X_b^{\text{SVC}}, X_1^{\text{SC}}, \ldots, X_c^{\text{SC}} \right] \tag{1}$$

Where, ***X*** represents the set of decision variables; Swich, SVC and SC represent connection switches, static var compensator and shunt capacitor; X_1^{Swich} and X_a^{Swich} represent the action states of the *1*-th and *a*-th connection switche respectively; X_1^{SVC} and X_b^{SVC} represent the compensation capacity of the *1*-th and *b*-th SVC; X_1^{SC} and X_c^{SC} represent the number of access groups of the *1*-th and *c*-th SC.

3.2. Objective functions

Economic benefit, energy loss and power quality are considered to optimize the operation of ADN, and the goal is to minimize the economic cost, active power loss and node voltage deviation.

3.2.1. Minimal economic cost

$$F_1 = \sum_{t=1}^{T} (C_a \sum_{k=1}^{N_b} P_{t.loss}^k + C_b N_S^t + C_r^t) \tag{2}$$

Where, *T*, *t* and *loss* represent total time, operating hours and power loss respectively; $P_{t.loss}^k$ and N_S^t represent the line active loss of the *k*-th branch in *t* period and the number of actions of the connecting switch in *t* period; N_b, C_a and C_b represent the number of branches, the operating loss coefficient and the unit action cost of the connection switch (this study sets C_b to \$10/time); and C_r^t represents the total operating cost of ADN in time *t*, including power purchase costs and equipment investment costs.

$$C_r^t = C_e^t (P_{load}^t - P_{DG}^t) + P \cdot \sum_{j=1}^{N_t} Q_t^j \cdot C_t^j \tag{3}$$

Where, *t*, *DG* and *load* represent operating hours, distributed generation and residential

load respectively; P_{DG}^{t} and P_{load}^{t} represent the total active power emitted by DG and the total load of ADN during *t* period; Q_{t}^{j} represents the compensation capacity of the *j*-th reactive power compensation device in the *t* period; C_{e}^{t}, C_{t}^{j} and N_{t} represent the electricity price, the unit compensation capacity investment cost of the *j*-th compensation equipment and the number of compensation equipment during the period *t*; and *P* represents the investment recovery coefficient.

The following is the investment recovery coefficient formula.

$$P=\frac{(1+a)^{y}\cdot a}{(1+a)^{y}-1} \tag{4}$$

Where, *a* and *y* represent interest rate and equipment service life. In this study, *a*=0.06, SVC life is set to 15 years and SC life is set to 20 years.

3.2.2. Minimum active power loss

$$F_{2}=\sum_{t=1}^{T}\sum_{k=1}^{N_b}R_{k}\frac{P_{t.k}^{2}+Q_{t.k}^{2}}{U_{t.k}^{2}} \tag{5}$$

Where, *T*, *k*, R_{k} and N_{b} represent total time, branch number, the resistance of the *k-th* branch and the quantity of branches; $P_{t.k}$ and $Q_{t.k}$ represent the injected active power and injected reactive power at branch *k* in period *t*; and $U_{t.k}$ represents the voltage amplitude at branch *k* in period *t*.

3.2.3. Minimum node voltage deviation

$$F_{3}=\sum_{t=1}^{T}\left(\frac{1}{N_{n}}\sum_{i=1}^{N_n}\left|U_{t.i}^{2}-U_{r}^{2}\right|\right) \tag{6}$$

Where, *t* and *T* represent the running time and total time respectively; N_{n}, U_{r} and $U_{t.i}$ represent the number of nodes, the reference voltage and the voltage amplitude at the *i*-th node during the *t* period.

3.3. Constraints

3.3.1. Power flow balance constraints

$$\begin{cases} P_{i}+P_{DG.i}=P_{load.i}+U_{i}\sum_{j=1}^{n}U_{j}(G_{ij}\cos\theta_{ij}+B_{ij}\sin\theta_{ij}) & i=1,2,...,N_{n} \\ Q_{i}+Q_{DG.i}=Q_{load.i}+U_{i}\sum_{j=1}^{n}U_{j}(G_{ij}\sin\theta_{ij}-B_{ij}\cos\theta_{ij}) & i=1,2,...,N_{n} \end{cases} \tag{7}$$

Where, *i* and *j* represent the start and end nodes of the branch respectively; N_{n}, *n*, *DG* and *load* represent total nodes, total branches, distributed generation and residential load respectively; P_{i} and Q_{i} represent the active and reactive power injected into *i*-th node;

$P_{DG.i}$ and $Q_{DG.i}$ represent the active and reactive power output by DG at the *i*-th node; $P_{load.i}$ and $Q_{load.i}$ represent the active and reactive power of load at the *i*-th node; U_i and U_j are the voltage of the *i*-th node and the voltage of the *j*-th node; and G_{ij}, θ_{ij} and B_{ij} represent the real part, impedance angle and imaginary part of the admittance between node *i* and node *j*.

3.3.2. Node voltage constraint

$$U_{i.\min} \le U_i \le U_{i.\max} \tag{8}$$

Where, $U_{i.\max}$, U_i and $U_{i.\min}$ represent the lower voltage limit, the present voltage and the upper voltage limit of the *i*-th node. $U_{i.\max}$ and $U_{i.\min}$ are taken as $1.05U_i$ and $0.9U_i$.

3.3.3. Branch current constraint

$$I_k \le I_{k.\max} \tag{9}$$

Where, I_k and $I_{k.\max}$ represent the current and the maximum current allowed to flow in the *k*-th branch.

3.3.4. SVC switching capacity constraint

$$Q_{svc.\min} \le Q_{svc} \le Q_{svc.\max} \tag{10}$$

Where, *SVC* represents static var compensator; $Q_{svc.\min}$, Q_{svc} and $Q_{svc.\max}$ represent the lower limit of SVC input capacity, input capacity and upper limit of SVC input capacity.

3.3.5. SC switching group number constraint

$$N_{SC.\min} \le N_{SC} \le N_{SC.\max} \tag{11}$$

Where, *SC* represents shunt capacitor; N_{SC} is the number of SC input groups; $N_{SC.\min}$ and $N_{SC.\max}$ are the upper and lower limits of the number of SC input groups.

3.3.6. Topological structure constraint

$$h \in H \tag{12}$$

Where, *h* and *H* represent the reconstructed network topology and feasible network topology set.

3.4. Simplification of network topology

This study uses a loop matrix to ensure the generation of decision variables that meet the radial structure of ADN. The elements of row in the loop matrix is composed of the connection switch numbers of an independent loop in the active distribution network topology, and then select a connection switch number from each row in the matrix to form a set of decision variables. In addition, the incidence matrix ***A*** (Azizivahed et al., 2017) is adopted to verify the radial topology.

The following are the steps to verify the radial structure.

Step 1. In the loop matrix, select one connection switch for each row to disconnect.

Step 2. Establish an incidence matrix $A_{n\times m}$ including all branches.

$$\boldsymbol{A}_{n\times m}=\begin{cases}1 & if\ \ I_n\ \ from\ \ N_m\\ -1 & if\ \ I_n\ \ to\ \ N_m\\ 0 & else\end{cases} \tag{13}$$

Where, *n* and *m* represent the branch number and node number respectively; I_n and N_m represent the current of the *n*-th branch and the *m*-th node respectively.

Step 3. Delete the row of $A_{n\times m}$ corresponding to the selected disconnect switch and the first column of $A_{n\times m}$ corresponding to the root node.

Step 4. If the remaining matrix determinant is -1 or 1, it is radial topology.

3.5. Multi-objective sparrow search algorithm and its application

ADN has complicated structure and numerous switches. The time-varying load and real-time electricity price need to be considered. Additionally, the increase of DG and reactive power compensation devices makes the optimization model more complicated. The proposed multi-objective sparrow search algorithm (MOSSA) is used to optimize the dynamic reconfiguration and reactive power collaborative optimization model of ADN for reducing the economic cost and energy waste and enhancing the power quality of ADN. Obtain Pareto front surface under different objective functions, and then get the optimal compromise solution through the technique for order preference by similarity to an ideal solution (TOPSIS).

This chapter improves sparrow search algorithm (SSA) by introducing non-dominated sorting, external archiving mechanism, third-order chaos initialization method, nonlinear decreasing population scale factor and Cauchy mutation method, and finally obtains MOSSA.

3.5.1. Sparrow search algorithm

Sparrow search algorithm (SSA) is an algorithm simulating the habits of sparrows, which has great optimization ability (Xue and Shen., 2020). The sparrow population is divided into discoverers and joiners, which are controlled by the population scale factor *W*. When aware of the danger, some sparrows with anti-predation behavior in the sparrow population are called scouts

(1) Discoverers

The discoverer has a wide range of foraging.

$$\boldsymbol{X}_i^{t+1}=\begin{cases}\boldsymbol{X}_i^{t}\times\exp(\dfrac{-i}{\alpha\times G}) & if\quad R_1<R_2\\ \boldsymbol{X}_i^{t}+Q\times\boldsymbol{L} & if\quad R_1\geq R_2\end{cases} \tag{14}$$

Where, $\boldsymbol{X}_i^{t+1}$ and $\boldsymbol{X}_i^{t}$ represents the position of the *i*-th sparrow at the *t*+1 and *t*-th iterations; *t*, *G*, and *Q* represent the current iteration number, the total iteration number and a number that obeys normal distribution; R_1 and R_2 are random numbers of [0,1] and [0.5,1], representing early warning value and safety value; α is a random number of (0,1]; $\boldsymbol{L}$ is a 1×*d* matrix with a value of 1 for each element; and *d* represents the variable dimension.

(2) Joiners

The joiner forages around the discoverer. The updated description of its location is as below.

$$\boldsymbol{X}_j^{t+1}=\begin{cases}\left|\boldsymbol{X}_b-\boldsymbol{X}_j^t\right|\times L\times \boldsymbol{A}+\boldsymbol{X}_b & if \quad i\le 0.5N\\ Q\times\exp(\dfrac{\boldsymbol{X}_w^t-\boldsymbol{X}_j^t}{j^2}) & if \quad i>0.5N\end{cases} \tag{15}$$

Where, $\boldsymbol{X}_b$ and $\boldsymbol{X}_w^t$ represent the position of the best and worst fitness sparrow; $\boldsymbol{X}_j^{t+1}$ and $\boldsymbol{X}_j^t$ represents the position of the *j*-th sparrow at the *t*+1 and *t*-th iterations; $\boldsymbol{A}$ is a 1×*d* matrix with a value of -1 or 1 for each element, and $\boldsymbol{A}=\boldsymbol{A}^T(\boldsymbol{A}\boldsymbol{A}^T)^{-1}$; $\boldsymbol{L}$ is a 1×*d* matrix with a value of 1 for each element; *d* and *Q* represent the variable dimension and a number that obeys normal distribution; and *j* represents the sparrow number.

(3) Scouters

$$\boldsymbol{X}_Z^{t+1}=\begin{cases}\boldsymbol{X}_Z^t+R\times(\dfrac{\left|\boldsymbol{X}_Z^t-\boldsymbol{X}_w^t\right|}{(f_b-f_w)+\varepsilon}) & if \quad f_Z\ge f_b\\ \boldsymbol{X}_b^t+\beta\times\left|\boldsymbol{X}_b^t-\boldsymbol{X}_Z^t\right| & if \quad f_Z<f_b\end{cases} \tag{16}$$

Where, $\boldsymbol{X}_Z^{t+1}$ and $\boldsymbol{X}_Z^t$ represent the positions of the *Z*-th scout at the (*t*+1)-th and *t*-th iterations; $\boldsymbol{X}_b^t$ and $\boldsymbol{X}_w^t$ represent the positions of the sparrows with the best fitness and the worst fitness at the *t*-th iteration; β is a random number with a normal distribution with a mean value of 0 and a variance of 1; f_w and f_b represent the global worst and optimal fitness values; f_Z represents the fitness value of the *z*-th individual; ε is a constant for avoiding the denominator being 0; and $R\in[-1,1]$ is a random number.

3.5.2. Multi-objective sparrow search algorithm

The multi-objective sparrow search algorithm (MOSSA) proposed in this study can optimize multiple objective functions by introducing non-dominated sorting mechanism and external archiving mechanism on the basis of SSA. Additionally, chaos initialization strategy, Cauchy mutation strategy and nonlinear decreasing population scale factor are introduced to increase population diversity, accelerate convergence speed and enhance search ability.

(1) Non-dominated sorting mechanism

For the minimization problem of *n* objective functions $f_n(x)$, if any two decision variables x_a and x_b satisfy equation (17), it is called x_a dominates x_b.

$$\exists f_k(x_a)<f_k(x_b)\,\|\,\forall f_k(x_a)\le f_k(x_b),\quad k\in\{1,2,\ldots,n\} \tag{17}$$

Where, x_a and x_b represent the *a*-th variable and *b*-th variable; $f_k(x)$ and *n* represent the *k*-th objective function and the number of objective functions.

(2) External archiving mechanism

MOSSA introduces an external archive to store the individual with the lowest Pareto

level in the iterative process. The update mechanism is as follows: 1) Compare the new solution with the solution in the archive. If the former is a non-dominated solution, the former is allowed to be stored in the archive; If the former dominates the latter, the former replaces the latter; and 2) If the archive exceeds the storage space, the congestion is calculated and the solution with high congestion is removed.

(3) Third-order chaotic initialization

The third-order chaotic mapping strategy is used to initialize the sparrow population. The initial solutions have the characteristics of uniform spatial distribution and randomness. The initialization formula is as follows.

$$\begin{cases} H_{i.(b+1)} = 4H_{i.b}{}^{3} - 3H_{i.b} \\ \boldsymbol{X}_{i.b} = (H_{i.b} + 1) \times \dfrac{u_b - l_b}{2} + l_b \\ i = 1, 2, \ldots, N_p \\ \left| H_{i.b} \right| \le 1 \end{cases} \tag{18}$$

Where, l_b and u_b represent the lower and upper limits of the *b*-dimensional variable ; $\boldsymbol{X}_{i.b}$ and N_p represent the *b*-th dimensional coordinate in the search space of the *i*-th individual and the population number; $H_{i.b}$ and $H_{i.(b+1)}$ represent the *b*-th and (*b*+1)-th dimensional coordinate of the *i*-th sparrow in the chaotic space.

(4) Nonlinear decreasing population scale factor

Early in MOSSA iteration, the current individual is usually far away from the global optimal solution. Increasing the value of population scale factor increases the proportion of discoverers, which is beneficial for the discoverers to perform global search. In the later stage of MOSSA iteration, reducing the value of population scale factor increases the proportion of joiners and give full play to the local search ability of joiners. The expression of the population scale factor *W* is as follows.

$$w = w_{\max} - \frac{\left(w_{\max} - w_{\min} \right) \times t}{T} \tag{19}$$

Where, *w*, *t*, *T*, $w_{\min}$ and $w_{\max}$ represent the population scale factor, the current number of iterations, the total number of iterations, the minimum value of *w* and the maximum value of *w*; and *w* nonlinearly changes from large to small as the iteration progresses.

(5) Cauchy mutation strategy

$$\boldsymbol{X}_{i.b}^{\mathrm{C}} = \boldsymbol{X}_{i.b} \cdot \left(1 + Cauchy \right) \tag{20}$$

$$Cauchy = \tan((\partial - 1/2) \cdot \pi) \tag{21}$$

$$\boldsymbol{X}_i = \begin{cases} \boldsymbol{X}_i & if\ \boldsymbol{X}_i\ domination\ \boldsymbol{X}_i^C \\ \boldsymbol{X}_i^C & else \end{cases} \tag{22}$$

Where, $\boldsymbol{X}_{i.b}$ and $\boldsymbol{X}_{i.b}^{C}$ are the *b*-th dimensional coordinates of the *i*-th sparrow before and after mutation; *Cauchy* is a Cauchy mutation operator; $\boldsymbol{X}_i$ and $\boldsymbol{X}_i^C$ are the *i*-th sparrow before and after mutation; and ∂ is a random variable on [0,1]. Perform a non-dominant

ranking with the individual before mutation, and determine the optimum individual by the method of survival of the fittest.

3.5.3. Adopting TOPSIS to select the optimal compromise solution

For multi-objective optimization problems, the objective functions may have contradictory relationships among them, and all objectives cannot reach the optimal values at the same time. Therefore, the multi-objective optimization algorithm obtains a set of optimal solution sets.

The technique for order of preference by similarity to ideal solution (TOPSIS) is a multi-criteria selection method that can efficiently select the optimal compromise solution from a set of optimal solutions (Singh et al., 2020). TOPSIS introduces the positive ideal solutions (PIS) and negative ideal solutions (NIS), and the optimal value of each objective function after normalization is used as the solution in PIS, and the worst value of each objective function is used as the solution in NIS. Then, the solution with the minimum geometric distance from PIS and the maximum geometric distance from NIS in the Pareto solution set is selected as the optimal compromise solution. This study uses TOPSIS to select a compromise solution from the Pareto optimal solution set obtained from MOSSA.

The steps for TOPSIS to choose the compromise solution are as follows.

Step 1. Establish normalized matrix $\boldsymbol{R}_{n_1\times n_2}$.

$$\boldsymbol{R}_{n_1\times n_2}=\begin{bmatrix} r_{1,1} & r_{1,2} & \cdots & r_{1,n_2} \\ r_{2,1} & r_{2,2} & \cdots & r_{2,n_2} \\ \vdots & \vdots & & \vdots \\ r_{n_1,1} & r_{n_1,2} & \cdots & r_{n_1,n_2} \end{bmatrix} \tag{23}$$

$$r_{i,j}=\frac{f_j(x^i)}{\sqrt{\sum_{l=1}^{n_1}\left[f_j(x^l)\right]^2}},\qquad j=1,2,...,n_2 \tag{24}$$

Where, n_1, n_2, $r_{i,j}$ and $f_j(x^i)$ represent the number of variables, the number of objective functions, the elements in the normalized matrix and the *j*-th function of the *i*-th solution; and $\boldsymbol{R}_{n_1\times n_2}$ is a normalized matrix.

Step 2. Determine positive ideal solution (PIS) and negative ideal solution (NIS).

$$\boldsymbol{PIS}=\left\{u_1^+,u_2^+,u_3^+,\cdots,u_{n_2}^+\right\} \tag{25}$$

$$\boldsymbol{NIS}=\left\{u_1^-,u_2^-,u_3^-,\cdots,u_{n_2}^-\right\} \tag{26}$$

$$\begin{cases} u_j^+=\min(r_{i,j}), & i=1,2,...,n_1, \quad j=1,2...n_2 \\ u_j^-=\max(r_{i,j}), & i=1,2,...,n_1, \quad j=1,2...n_2 \end{cases} \tag{27}$$

Where, $r_{i,j}$, ***PIS*** and ***NIS*** represent the elements in the normalized matrix, the positive ideal solution and negative ideal solution; u_j^+ and u_j^- represent the *j*-th ***PIS*** and ***NIS***.

Step 3. Calculate distance and approximate degree.

$$\begin{cases} d_i^+ = \sqrt{\sum_{j=1}^{n_2} (r_{i,j} - u_j^+)^2} \\ d_i^- = \sqrt{\sum_{j=1}^{n_2} (r_{i,j} - u_j^-)^2} \end{cases} \tag{28}$$

$$C_i = \frac{d_i^-}{d_i^+ + d_i^-} \tag{29}$$

Where, C_i, d_i^+ and d_i^- represent the degree of similarity, the distance from the *i*-th solution to ***PIS*** and ***NIS***; and select the solution with the largest *C* value as the final selected compromise solution; u_j^+ and u_j^- represent the *j*-th ***PIS*** and ***NIS***; and $r_{i,j}$ represents the elements in the normalized matrix.

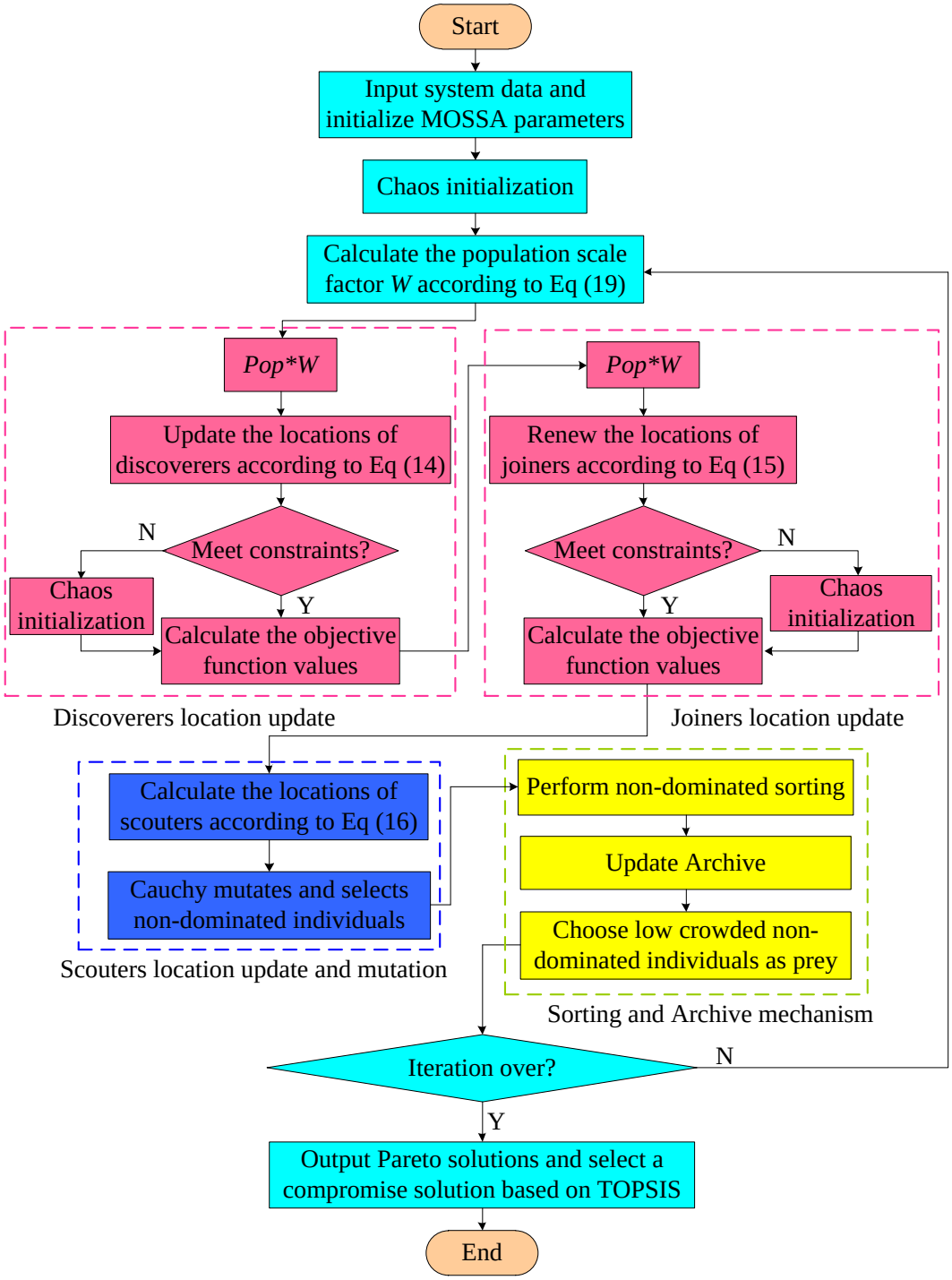

Figure 1. Flow chart of MOSSA optimized ADN dynamic reconfiguration and reactive power collaborative optimization model

The process of MOSSA optimizing ADN dynamic reconfiguration and reactive power collaborative optimization model is shown in Figure 1.

4. Case analysis and Test

Firstly, in two independent studies of solving the test function and optimizing the proposed model, MOSSA is compared with current algorithms to verify the superiority. Secondly, to verify the effectiveness of the proposed model, a comparative analysis is

conducted under the four scenarios of IEEE 33 system.

4.1. Multi-objective sparrow search algorithm performance evaluation

Multi-objective particle swarm optimization (MOPSO), non-dominated sorting genetic algorithm with elite strategy (NSGA-II), non-dominated sorting moth flame optimization (NSMFO) and multi-objective gray wolf optimization (MOGWO) algorithm are the latest proposed or classical excellent multi-objective optimization algorithms. NSMFO is an excellent multi-objective algorithm that imitates the life habits of moths (Sapre et al., 2021). NSGA-II (Zhang et al., 2021) and MOPSO (Tavana et al., 2016) are classical algorithms and usually used as a comparison algorithm. MOGWO is a multi-objective algorithm with strong search capability (Mirjalili et al., 2016). Therefore, this study selects NSMFO, NSGA-II, MOPSO and MOGWO as the comparison algorithms. The parameters of each comparison algorithm in Table 2 refer to the mentioned literature.

Select zero-ductility transition (ZDT) series classic test function (Mirjalili et al., 2017) to test the performance of multi-objective sparrow search algorithm (MOSSA), and compare the test results with MOPSO, NSGA-II, NSMFO and MOGWO.

4.1.1. Standard test function and performance evaluation index

The zero-ductility transition (ZDT) series functions have Pareto optimal frontiers with different shapes, and the parameters are shown in Table 1.

Table 1. ZDT series test functions

Function	ZDT1	ZDT2	ZDT3	ZDT4	ZDT6
Variable dimension	30	30	30	10	10
Spatial dimension	2	2	2	2	2
Concave and convex	convexity	concavity	concavity	convexity	concavity
Continuity	continuity	continuity	discontinuity	multiplex mode	continuity

During the experiment, to ensure the objectivity of the results, the main parameters of all algorithms are as below: population size N=100, external archive size *Archive*=100 and maximum number of iterations $T_{\max}$=100. Table 2 shows the parameters of the NSMFO, NSGA-II, MOPSO, MOGWO and MOSSA algorithms.

Table 2. Parameter settings for five optimization algorithms

Algorithms	Parameters
NSMFO	N=100, T_{max}=100, b=1
NSGA-II	N=100, T_{max}=100, P_C=0.9, P_m=0.5, m_s=0.05
MOPSO	N=100, T_{max}=100, C_1=2, C_2=2, w=0.3, U_p=0.5
MOGWO	N=100, T_{max}=100, b_t=4, g_m=2
MOSSA	N=100, T_{max}=100, $W_p \in$[0.2, 0.7], R_2=0.7, SD=0.1

The population size of each algorithm is N=100, the number of iterations T_{max}=100 and the external archive size *Archive*=100. In NSMFO, b is the spiral parameter. In NSGA-II, P_C, P_m,

and m_s represent the crossover probability, mutation probability and mutation strength. In MOPSO, C_1, C_2, w and U_p represent self-learning factor, social cognitive factor, inertia weight and percentage of uniform weight, respectively. In MOGWO, b_t and g_m represent leader selection pressure parameter and removal pending member selection pressure. In MOSSA, W_p, R_2 and SD represent population proportion factor, safety value and warning individual proportion, respectively.

Inverted generational distance (IGD) is the Euclidean distance average of each reference point to the nearest solution, which reflects the approximation of the whole solution set to the reference set (Jiang et al., 2016). It is used to evaluate the convergence accuracy of the algorithm, and the smaller its value indicates the higher convergence accuracy of the algorithm. Spacing (SP) reflects the extensive degree of the whole solution set in the target space (Li et al., 2016). It is desired that the resulting solution set is widely distributed in space, so the SP indicator is chosen to measure the degree of distribution of the obtained solution set in space. Smaller SP value indicates more uniform spatial distribution of the solution set. Hypervolume (HV) is the volume of the space enclosed by the solution set and the reference points. It evaluates both the algorithm convergence and the diversity of solutions, and a larger value indicates a better comprehensive performance of the algorithm. CPU runtime is used to evaluate the computational speed of the algorithm.

Therefore, IGD, SP, HV and CPU runtime are introduced as algorithm evaluation indicators to compare the property of different optimization algorithms. The corresponding calculation formula is as follows.

$$IGD(\boldsymbol{P}, \boldsymbol{P}_t) = \frac{\sum_{x \in P_t, y \in p} \min\{\mathrm{dis}(x, y)\}}{N_t} \tag{30}$$

$$SP = \left(\frac{1}{N-1} \times \sum_{j=1}^{N} \left(d_j - \bar{d} \right)^2 \right)^{1/2} \tag{31}$$

$$HV = \chi \sum_{i=1}^{N} V_i \tag{32}$$

Where, *IGD*, *SP* and *HV* represent the inverted generational distance, spacing and hypervolume; $\boldsymbol{P}_t$, $\boldsymbol{P}$ and N_t are the actual Pareto front surface, the calculated Pareto solution set and the number of solutions in $\boldsymbol{P}_t$; d_j, N, and $\bar{d}$ represent the minimum distance from the j-th solution to other solutions, the number of solutions in $\boldsymbol{P}$ and the mean value of d_j; $\mathrm{dis}(x, y)$ represents the distance between x and y; and χ, V_i represent the Lebesgue measure and the hypervolume formed by the i-th solution and the reference point, respectively.

The smaller values of IGD and SP represent faster convergence and better spatial distribution of the obtained solution sets, respectively. Shorter CPU runtime means faster algorithm computation. The higher values of HV represent better convergence and diversity of solutions, and better overall performance of the algorithm.

4.1.2. Analysis of test function results

Each algorithm runs 30 times independently to ensure the objectivity and the evaluation index is the average of the results of 30 runs. To ensure the objectivity of the results, the population size of all algorithms is N=100, the number of iterations is T_{max}=100 and the external archive size is *Archive*=10*0*. The average values of IGD, SP, HV and CPU runtime of different algorithms on the test function are shown in Table 3, Table 4, Table 5 and Table 6. Figure 2, Figure 3 and Figure 4 show the Pareto frontiers of the five algorithms on each test function.

Table 3. IGD test results

Method	ZDT1	ZDT2	ZDT3	ZDT4	ZDT6
NSMFO	1.38E-02	1.03E-02	2.88E-01	2.26E-01	1.15
NSGA-II	1.54E-02	5.02E-02	3.06E-02	4.07	4.21E-03
MOPSO	1.55E-02	1.42E-02	2.28E-02	94.53	2.82E-02
MOGWO	6.55E-03	5.98E-03	9.40E-03	3.69	5.57E-03
MOSSA	**3.17E-03**	**3.43E-03**	**3.49E-03**	**3.31E-03**	**2.56E-03**

In Table 3, the bold font is the optimal value. Compared with NSMFO, NSGA-II, MOPSO and MOGWO, the MOSSA proposed in this study has obtained the best IGD on the all test functions. The MOSSA has the best convergence. The IGD of NSGA-II, MOPSO and MOGWO on the ZDT4 test function is too large, which is not in the same order of magnitude as the IGD of MOSSA. In the ZDT4 test function, under the condition of 100 iterations, NSGA-II, MOPSO and MOGWO all fall into local optimum, and optimal Pareto solution set cannot be found. The IGD of NSMFO under the ZDT6 test function is also too large and it falls into local optimum. However, the MOSSA can obtain the optimal Pareto solution set under all test functions. The MOSSA has strong search ability and the fastest convergence speed.

Table 4. SP test results

Method	ZDT1	ZDT2	ZDT3	ZDT4	ZDT6
NSMFO	7.51E-02	8.43E-03	5.90E-02	7.29E-02	3.95E-02
NSGA-II	8.98E-03	2.53E-02	1.53E-02	3.92E-01	7.26E-03
MOPSO	6.50E-03	9.42E-03	1.25E-02	9.75E-02	1.75E-01
MOGWO	8.05E-03	6.49E-03	1.18E-02	1.60E-01	**5.55E-03**
MOSSA	**4.51E-03**	**4.57E-03**	**4.74E-03**	**4.68E-03**	1.63E-01

The bold font in Table 4 is the optimal value of SP under each test function. By comparing and analyzing the SP indicators, the MOSSA obtained four optimal SP values on the five test functions, MOGWO has obtained one optimal SP value, and other algorithms have not obtained the optimal value. The spatial distribution of MOSSA solution is better, and its performance is only next to the NSMFO in the ZDT6 test function. The Pareto solution set obtained by MOSSA has a better spatial distribution.

Table 5. HV test results

Method	ZDT1	ZDT2	ZDT3	ZDT4	ZDT6

NSMFO	6.46E-01	3.10E-01	9.54E-01	6.61E-01	0
NSGA-II	6.45E-01	2.97E-01	1.009	5.09E-01	3.20E-01
MOPSO	6.26E-01	2.98E-01	9.76E-01	0	3.08E-01
MOGWO	6.57E-01	3.27E-01	1.024	0	3.20E-01
MOSSA	**6.62E-01**	**3.29E-01**	**1.043**	**6.62E-01**	**3.23E-01**

Table 5 shows the HV test results of each algorithm under different test functions, where the bolded font is the HV optimum. the HV values of MOPSO and MOGWO are zero under the ZDT4 test function, and the HV value of NSMFO is also zero under the ZDT6 test function, they converge slowly and cannot find the Pareto optimal solution set in the multi-modal complex test function. Compared with NSMFO, NSGA-II, MOGWO and MOPSO, the proposed MOSSA obtains the optimal HV values under all test functions. MOSSA has the best convergence, the best solution diversity and the best comprehensive performance of the algorithm.

Table 6. CPU runtime

Method	ZDT1	ZDT2	ZDT3	ZDT4	ZDT6
NSMFO	9.21	9.50	10.29	9.15	11.91
NSGA-II	2.02	2.60	2.03	3.15	2.75
MOPSO	**1.49**	**1.51**	**1.28**	2.82	**1.47**
MOGWO	106.68	95.12	78.88	8.76	116.23
MOSSA	1.93	2.14	2.11	**1.63**	1.64

Table 6 shows the CPU running time of each algorithm under each test function, and the bolded font is the minimum CPU running time. MOPSO is the quickest in the ZDT1, ZDT2 and ZDT3 test function, but the search ability is insufficient, and it is easy to fall into local optimum, and the convergence speed and convergence accuracy are inferior to MOSSA. MOGWO is the slowest in the ZDT series test function, and it is easy to fall into local optimum in the complex multi-modal test function. MOSSA has the shortest CPU running time only under ZDT4 test function, but the calculating time in other test functions is little different from the optimal value, usually only second to the optimal value, and the convergence speed is the fastest, the accuracy is the highest, the spatial distribution of the solution is the best, and the algorithm has the best comprehensive performance.

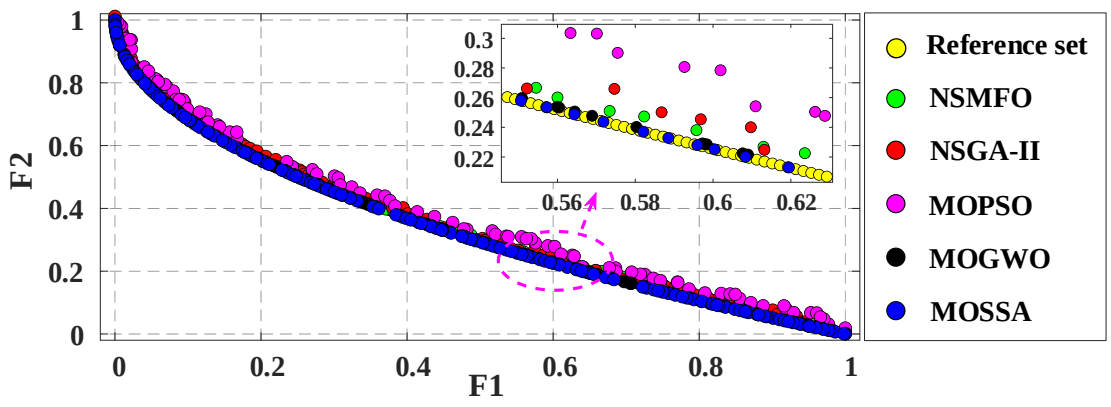

(a) ZDT1 test result

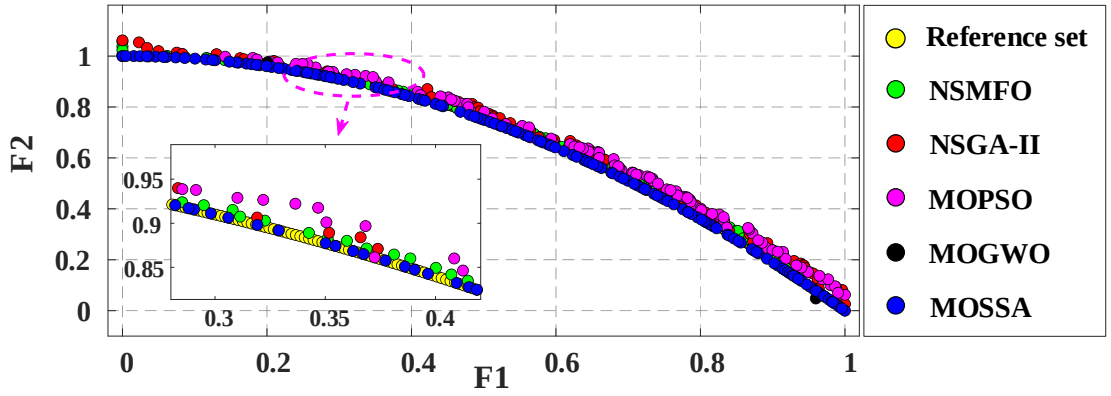

(b) ZDT2 test result

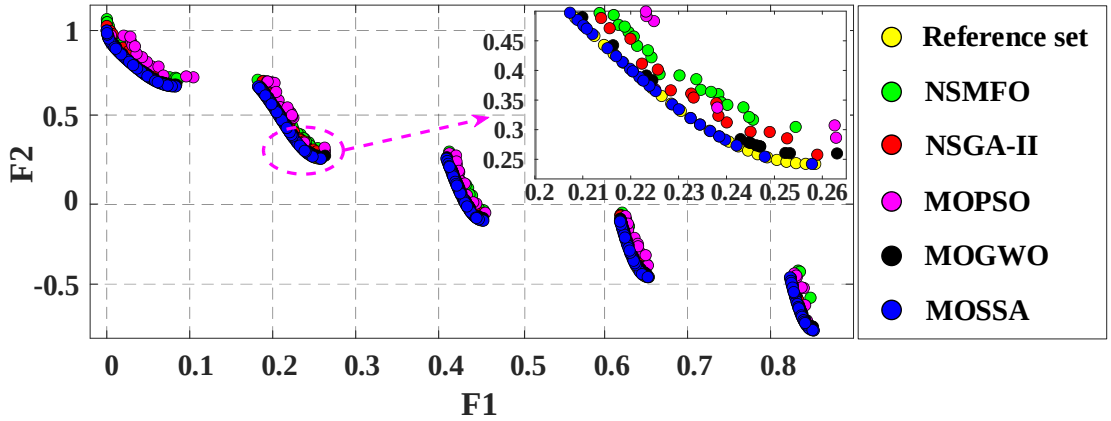

(c) ZDT3 test result.

Figure 2. Test results of each algorithm in ZDT1, ZDT2 and ZDT3

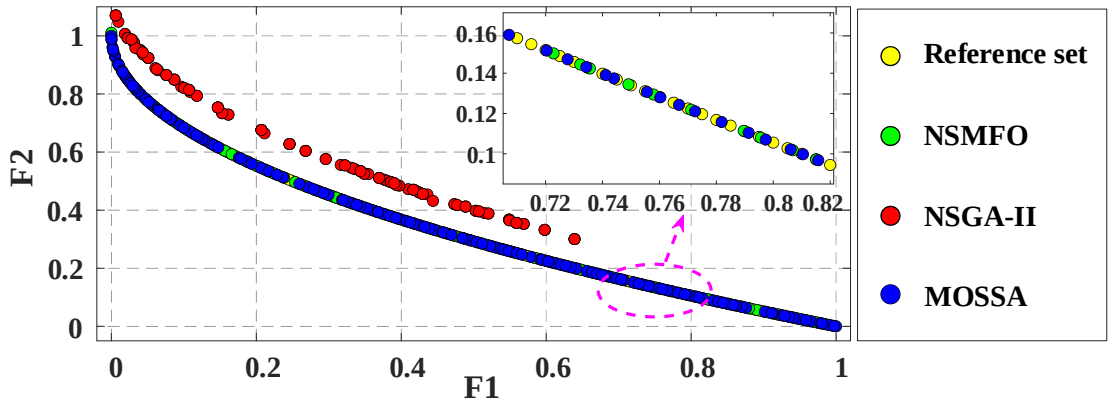

(a) ZDT4 test result of NSMFO, NSGA-II and MOSSA

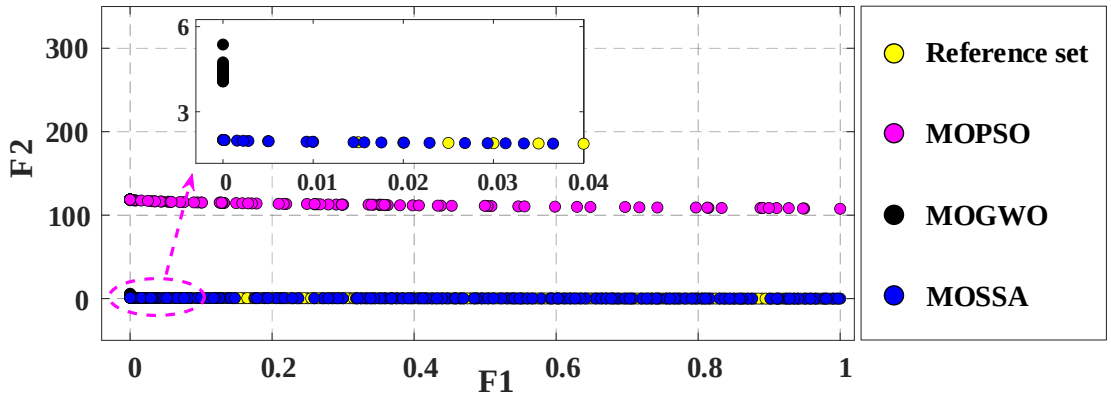

(b) ZDT4 test result of MOPSO, MOGWO and MOSSA

Figure 3. ZDT4 test results

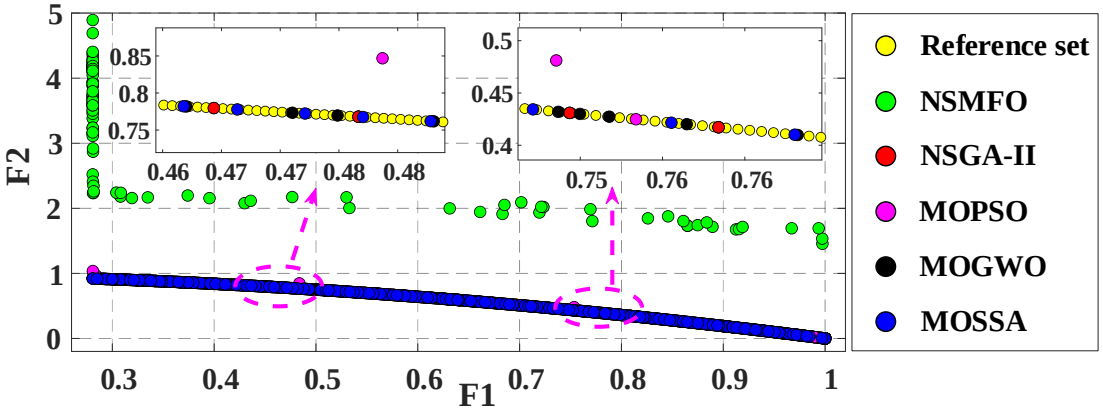

Figure 4. ZDT6 test results

Figure 2 indicates that in solving simple multi-objective problems, NSMFO, NSGA-II, MOPSO, MOGWO and MOSSA can all find the Pareto optimal frontier. But compared with NSMFO, NSGA-II, MOPSO and MOGWO, the solution of MOSSA is closer to the real frontier and the distribution is more uniform. The convergence and solution distribution of the MOSSA is the best.

In Figure 3, MOPSO cannot find the real Pareto front surface under the ZDT4 test function, MOGWO falls into a local optimum and the Pareto solution set found by NSGA-II contains too few solutions. The solutions found by NSMFO and MOSSA are all on the real frontier, but in combination with Table 3 and Table 4, it can be found that the performance of MOSSA is better than NSMFO. The MOSSA can find the real Pareto front surface in solving the problem of multi-modal complex functions, and the convergence and solution distribution are better than NSMFO, NSGA-II, MOPSO and MOGWO.

In Figure 4, NSMFO has not yet converged to the real Pareto front surface under the ZDT6 test function, and the solutions of NSGA-II, MOPSO, MOGWO and MOSSA are all on the real Pareto front surface. However, combined with Table 3, the MOSSA has better convergence than NSMFO, NSGA-II, MOPSO and MOGWO.

4.1.3. Friedman test and post-hoc Nemenyi test

Friedman test (Carrasco et al., 2020) and post-hoc Nemenyi test (Derrac et al., 2014) are used to compare the results of IGD, SP and HV indexes obtained by each algorithm respectively.

Friedman test is the non-parametric test to achieve the purpose of the analysis of variance test. The original hypothesis of this study assumes that none of the algorithm metrics are significantly different, and the alternative hypothesis assumes that the algorithm metrics are significantly different. When the original hypothesis is rejected, it indicates that the algorithms perform significantly differently, and post-hoc Nemenyi test is performed at this time. The post-hoc Nemenyi test is to compare the difference between the mean ordinal values of the algorithms with the critical difference (CD), and if it is greater than CD, then the algorithm with the higher mean rank is statistically superior to the algorithm with the lower rank. Conversely, there is no difference between the algorithms. The formula for CD is

$CD = q.\sqrt{k(k+1)/(6N)}$, *K* is the number of algorithms and *N* is the number of data sets. The *q* of this study is 2.459, five algorithms and five data sets are tested statistically, so the *CD* value is 2.459.

Table 7. *P*-values of IGD, SP and HV Indicators obtained by each algorithm

Indicators	IGD	SP	HV
P-value	6.63E-02	1.04E-01	1.04E-02

Table 7 shows the *P*-values of IGD, SP, HV indicators obtained by each algorithm, where the *P*-values of IGD and HV indicators are less than 0.01, indicating that the original hypothesis is rejected and there is a significant difference in the value of each test function of IGD and SP obtained by the algorithm, while the *P*-value of SP indicator is greater than 0.01 and the original hypothesis is accepted and there is no significant difference between the value of each test function in the SP indicator obtained by the algorithm.

Table 8. Average sequential values of each algorithm on different indicators

Indicators	NSMFO	NSGA-II	MOPSO	MOGWO	MOSSA
IGD	3.4	3.8	4	2.2	1.6
SP	3.6	4	3.4	2.4	1.6
HV	**2.4**	**2.5**	**1.7**	3.4	5

Table 8 shows the average sequential values of each algorithm on different indicators. The bolded font shows the data where the difference between the average sequence of the other algorithms and MOSSA is greater than the CD value. There is no significant difference between the IGD and SP metrics obtained by each algorithm in each test function. Among the HV metrics obtained under each test function, MOSSA statistically outperforms NSMFO, NSGA-II and MOPSO and it is not significantly different from MOGWO. Although there is no significant difference in IGD and SP metrics, combining Tables 3 and 4, MOSSA has the best IGD value in all tested functions, and the SP value is only second to MOGWO in the ZDT6 function, and the best SP value is obtained in all other functions. MOSSA outperforms all other compared algorithms.

4.2. IEEE 33 test system and its parameters

This study selects the IEEE 33 system as the test system. The total load, reference capacity and reference voltage of the system are 3715+j2350kVA, 10MVA and 12.66kV. There are 37 branches in the original network (including five tie-line branches). The distribution network generally operates in an open loop state, so five tie-lines are disconnected during normal system operation. The distribution system is a radial distribution network structure composed of 32 branches. System parameters are default parameters (Tolabi et al., 2020). Table 9 shows the parameters of the IEEE 33 system.

Table 9. IEEE 33 system parameters

Branch	Impedance (Ω)	Apparent	Branch	Impedance (Ω)	Apparent power

		power (kVA)			(kVA)
1	0.0922+j0.0470	100+j60	20	0.4095+j0.4784	90+j40
2	0.4930+j0.2511	90+j40	21	0.7089+j0.9373	90+j40
3	0.3660+j0.1864	120+j80	22	0.4512+j0.3083	90+j50
4	0.3811+j0.1941	60+j30	23	0.8980+j0.7091	420+j200
5	0.8190+j0.7070	60+j20	24	0.8960+j0.7011	420+j200
6	0.1872+j0.6188	200+j100	25	0.2030+j0.1034	60+j25
7	0.7114+j0.2351	200+j100	26	0.2842+j0.1447	60+j25
8	1.0300+j0.7400	60+j20	27	1.0590+j0.9337	60+j20
9	1.0440+j0.7400	60+j20	28	0.8042+j0.7006	120+j70
10	0.1966+j0.0650	45+j30	29	0.5075+j0.2585	200+j600
11	0.3744+j0.1238	60+j35	30	0.9744+j0.9630	150+j70
12	1.4680+j1.1550	60+j35	31	0.3105+j0.3619	210+j100
13	0.5416+j0.7129	120+j80	32	0.3410+j0.5362	60+j40
14	0.5910+j0.5260	60+j10	33	2.00+j2.00	0+j0
15	0.7463+j0.5450	60+j20	34	2.00+j2.00	0+j0
16	1.2890+j1.7210	60+j20	35	2.00+j2.00	0+j0
17	0.3720+j0.5740	90+j40	36	0.50+j0.50	0+j0
18	0.1640+j0.1565	90+j40	37	0.50+j0.50	0+j0
19	1.5042+j1.3554	90+j40			

The first node in the system is the root node, and the 5-th and 16-th nodes have photovoltaic (PV) access. The PV installed capacity is 500kW. The constant power factor control method is adopted during operation and the power factor is set to 0.85 (lagging). The 12-th node has wind turbine (WT) access. The installed capacity of the WT is 500kW. The constant power factor control method is adopted during operation and the power factor is set to 0.9 (lagging). One static var compensator (SVC) is installed at node 7 and two shunt capacitors (SC) are installed at node 21 and node 30 respectively. The improved IEEE 30 system topology is shown in Figure 5. The photovoltaic output power of the DKASC power station on September 6, 2015 is selected as the PV output power. The WT output prediction data (Guimaraes et al., 2021) is selected as the WT output power. Figure 6 shows the variation curve of load and DG. The load of each period of nodes in the system is the load of each node multiplied by the load unit value of this period. Table 10 shows real-time electricity prices.

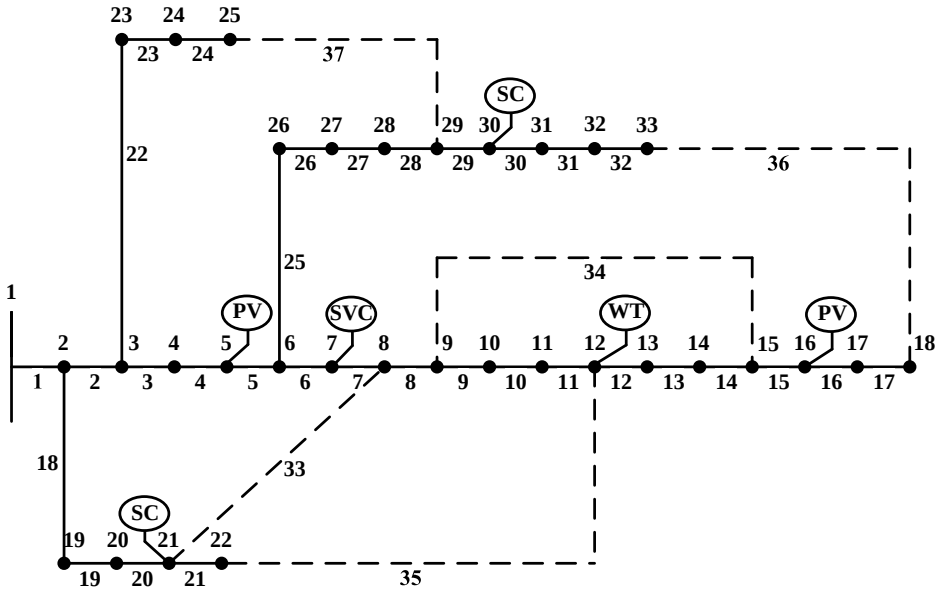

Figure 5. Improved IEEE30 system topology diagram

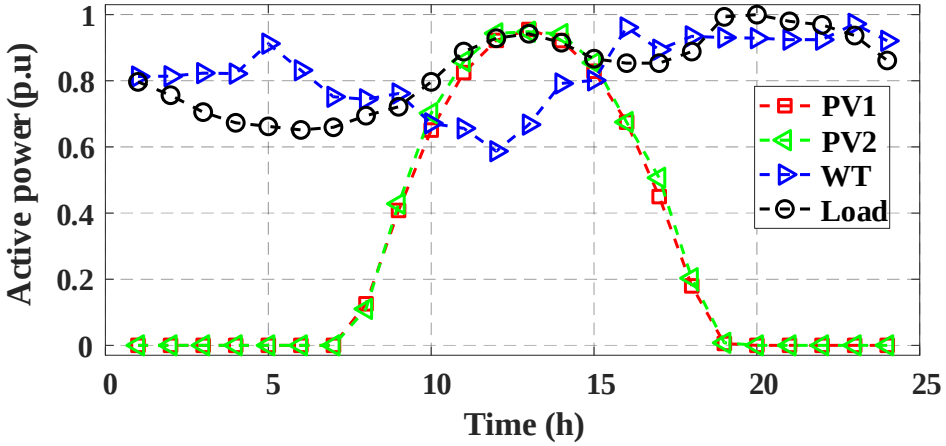

Figure 6. Load and DGs output active power per unit value in each period

Table 10. Real-time electricity price list

	Unit price ($/kWh)	Time period
Electricity	0.0547	23:00-7:00
	0.1285	7:00-10:00, 15:00-16:00, 17:00-18:00, 21:00-23:00
	0.2000	10:00-11:00, 13:00-15:00, 18:00-21:00
	0.2252	11:00-13:00, 16:00-17:00

4.3. Algorithm performance analysis

The time when PV output is the largest (13 o'clock) is selected for analysis to verify the superiority of the multi-objective sparrow search algorithm (MOSSA) in optimizing the proposed model.

In IEEE 33 system, compare with non-dominated sorting moth flame optimization (NSMFO), non-dominated sorting genetic algorithm with elite strategy (NSGA-II),

multi-objective multi-verse optimization (MOMVO) and multi-objective sparrow search algorithm (MOSSA) under different scenarios. In IEEE 33 system, aiming to ensure the fairness of the comparisons, the population size of all algorithms is N=50, the number of iterations is T_{max}=150, and the external profile size is *Archive*=50, and other parameters of each algorithm are shown in Table 2.

4.3.1. Optimization of multi-dimensional objective functions by different algorithms

Figure 7 shows the Pareto front surface obtained by NSMFO, NSGA-II, MOMVO, and MOSSA with different objective functions. Table 11 to Table 14 list the best compromise solutions selected by different algorithms through technique for order preference by similarity to ideal solution (TOPSIS) in the Pareto solution set of different objective functions.

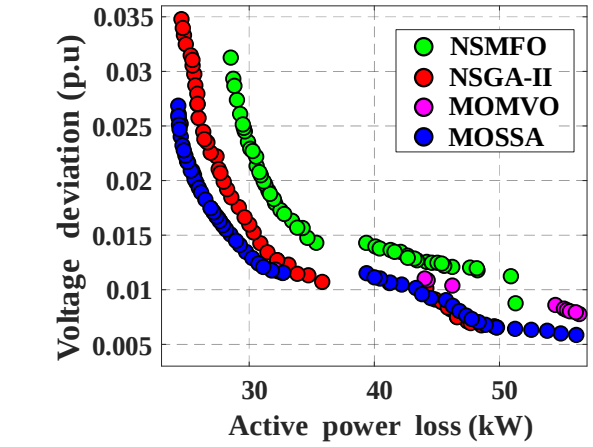

(a) Voltage deviation and power loss

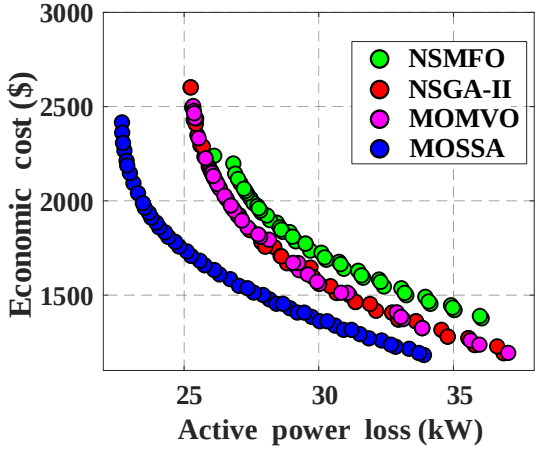

(b) Economic cost and power loss

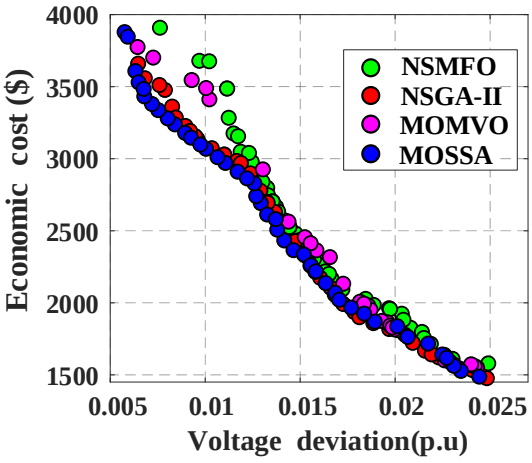

(c) Economic cost and voltage deviation

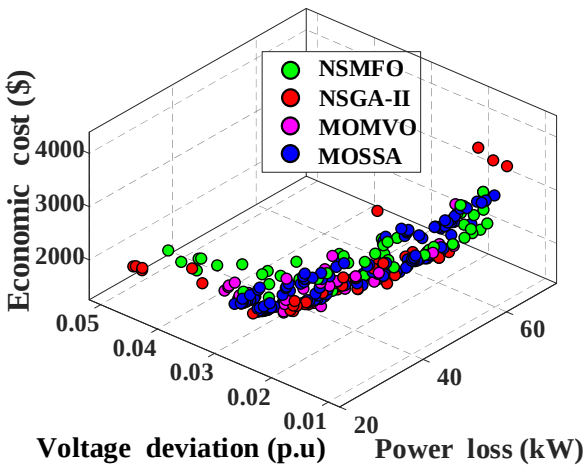

(d) Consider three objective functions

Figure 7. The optimization results of multi-dimensional objective functions of algorithms

In Figure 7, the Pareto front surface obtained by the MOSSA is closer to the origin than NSMFO, NSGA-II and MOMVO when considering two objective functions. The MOSSA has better convergence and solution set. The three-dimensional Pareto front surface obtained by MOSSA is a spatial surface, and the three goals of network loss, voltage deviation and economic cost have a strong coupling relationship. The solution set obtained by MOSSA contains more solutions than NSMFO, NSGA-II and MOMVO, and the performance of the MOSSA is better.

Table 11. The compromise solution obtained by each algorithm with active power loss and voltage deviation as goals

Method	Open switches	$\{Q_{svc}\}^{node}$ (kVar)	$\{N_{sc}\}^{node}$	SP	Power loss (kW)	Voltage deviation (p.u)
NSMFO	[4,11,21,30,27]	$\{730\}^{7}$	$\{2\}^{21}$ $\{19\}^{30}$	**2.12E-01**	35.36	1.43E-02
NSGA-II	[7,9,21,31,28]	$\{180\}^{7}$	$\{8\}^{21}$ $\{19\}^{30}$	6.84E-01	33.84	**1.14E-02**
MOMVO	[6,14,9,31,28]	$\{490\}^{7}$	$\{15\}^{21}$ $\{20\}^{30}$	5.60E-01	32.66	1.15E-02
MOSSA	[6,14,9,31,28]	$\{640\}^{7}$	$\{10\}^{21}$ $\{20\}^{30}$	3.36E-01	**31.81**	1.17E-02

Table 12. The compromise solution obtained by each algorithm with active power loss and economic cost as goals

Method	Open switches	$\{Q_{svc}\}^{node}$ (kVar)	$\{N_{sc}\}^{node}$	SP	Power loss (kW)	Economic cost ($)
NSMFO	[5,13,9,15,27]	$\{40\}^{7}$	$\{1\}^{21}$ $\{6\}^{30}$	8.48	31.64	1.592E+03
NSGA-II	[5,34,9,14,28]	$\{30\}^{7}$	$\{0\}^{21}$ $\{6\}^{30}$	20.50	31.36	1.464E+03
MOMVO	[5,34,8,14,28]	$\{0\}^{7}$	$\{0\}^{21}$ $\{7\}^{30}$	18.79	30.83	1.513E+03
MOSSA	[7,12,9,31,3]	$\{0\}^{7}$	$\{0\}^{21}$ $\{6\}^{30}$	**6.91**	**28.43**	**1.454E+03**

Table 13. The compromise solution obtained by each algorithm with voltage deviation and economic cost as goals

Method	Open switches	$\{Q_{svc}\}^{node}$ (kVar)	$\{N_{sc}\}^{node}$	SP	Voltage deviation (p.u)	Economic cost ($)
NSMFO	[4,34,35,31,28]	$\{320\}^{7}$	$\{7\}^{21}$ $\{10\}^{30}$	35.22	1.44E-02	2.526E+03
NSGA-II	[4,34,10,29,28]	$\{280\}^{7}$	$\{6\}^{21}$ $\{20\}^{30}$	24.83	1.73E-02	**1.992E+03**
MOMVO	[4,12,35,32,28]	$\{50\}^{7}$	$\{4\}^{21}$ $\{18\}^{30}$	82.14	1.44E-02	2.564E+03
MOSSA	[4,9,35,31,28]	$\{440\}^{7}$	$\{1\}^{21}$ $\{10\}^{30}$	**13.72**	**1.41E-02**	2.433E+03

Table 14. The compromise solution of each algorithm with active power loss, voltage deviation and economic cost as goals

Method	Open switches	$\{Q_{svc}\}^{node}$ (kVar)	$\{N_{sc}\}^{node}$	SP	Power loss (kW)	Voltage deviation (p.u)	Economic cost ($)
NSMFO	[4,9,35,31,28]	$\{210\}^{7}$	$\{7\}^{21}$ $\{13\}^{30}$	22.87	41.83	**1.45E-02**	2.601E+03
NSGA-II	[7,14,9,31,28]	$\{0\}^{7}$	$\{0\}^{21}$ $\{1\}^{30}$	36.53	29.56	2.30E-02	**1.953E+03**
MOMVO	[7,14,21,32,28]	$\{20\}^{7}$	$\{0\}^{21}$ $\{20\}^{30}$	57.45	**26.60**	2.25E-02	2.225E+03
MOSSA	[7,11,21,32,28]	$\{200\}^{7}$	$\{4\}^{21}$ $\{12\}^{30}$	**9.29**	29.63	2.04E-02	2.268E+03

Table 11 shows the compromise solution obtained by NSMFO, NSGA-II, MOMVO and MOSSA with voltage deviation and power loss as the target, and the font of the optimal value of each index is bold. The compromise solution obtained by MOSSA has the smallest power loss. Although the voltage deviation of the compromise solution obtained by MOSSA is not as good as that obtained by NSGA-II, they are all on the same order of magnitude. The

SP obtained by MOSSA is second to NSMFO, but in conjunction with Figure 7(a), the Pareto solution set of MOSSA is the closest to the origin and the algorithm has the best convergence.

Table 12 shows the compromise solution obtained by NSMFO, NSGA-II, MOMVO and MOSSA with power loss and economic cost as the target. The bold font is the optimal value of each index. Compared with NSMFO, NSGA-II and MOMVO, the MOSSA has the lowest power loss, economic cost and SP value. The compromise solution of MOSSA has the optimal value of each goal, and the Pareto solution set of MOSSA has the most uniform distribution. Combined with Figure 7(b), the Pareto front obtained by MOSSA is closest to the origin, it has the best convergence, and each index is the best.

Table 13 shows the compromise solution obtained by NSMFO, NSGA-II, MOMVO and MOSSA for minimizing voltage deviation and economic cost, and the font of the optimal value of each index is bolded. The compromise solution obtained by MOSSA has the smallest voltage deviation and its only inferior to the compromise solution obtained by NSGA-II in the cost index. Compared with the NSMFO, NSGA-II and MOMVO, the SP obtained by MOSSA has the smallest value. The solution set distribution of MOSSA is the most uniform.

Table 14 shows the compromise solution obtained by NSMFO, NSGA-II, MOMVO and MOSSA with active power loss, voltage deviation and economic cost as the target. The bold font is the optimal value of each indicator. Compared with NSMFO, NSGA-II, and MOMVO, the MOSSA has the smallest value of SP. The solution set distribution of MOSSA is the most uniform. The compromise solution obtained by NSMFO has the optimal value in the voltage deviation, but the power loss and economic cost are higher than MOSSA. The compromise solution of NSGA-II obtains the smallest economic cost, but the voltage deviation is higher than the compromise solution of MOSSA. The compromise solution obtained by MOMVO has the lowest active power loss. The compromise solution obtained by MOSSA is more balanced in the target of active power loss, economic cost and voltage deviation. Using the MOSSA to optimize the model proposed in this study for dynamic reconfiguration and reactive power collaborative optimization of ADN can consider various goals and obtain a comprehensive optimal solution.

In addition, this study compares the optimization results of the proposed MOSSA for ADN with those of the latest methods applied to ADN optimization. For example, Ji et al. (2021) proposes the improved second-order cone program (ISOCP), Nguyen et al. (2019) proposes the improved cuckoo search algorithm (ICSA), Jafari et al. (2020) proposes the exchange market algorithm and wild goats algorithm ((EMA-WGA), and Tolabi et al. (2020) proposes the thief and police algorithm (TPA).

In the initial state of the system, the power loss is 196.60kW, the node voltage deviation is 0.0995 p.u, and the voltage minimum is 0.91 p.u. The ISOCP reduces the power loss to 91.22kW and the voltage deviation to 0.0499 p.u. The ICSA reduces the power loss to 139.55kW and the voltage minimum is 0.9378 p.u. The EWA-WGA reduces the power loss to 142.42kW. The TPA reduces the power loss to 22.14kW and the operating cost to 38,590$. The proposed MOSSA reduces the power loss to 29.63kW, the voltage deviation to 0.0204 p.u, and the economic cost to 2268$. The optimization results show that the performance of

the proposed method is better than the methods proposed in the latest literature, further verifying the effectiveness of the proposed method.

4.4. Model performance analysis

This study evaluates the IEEE 33 test system in terms of energy saving, power quality, and economic benefits. Three performance parameters, including total power loss, total node voltage deviation and total economic cost, are used to evaluate the IEEE 33 test system using the optimized technique. Total power loss measures the system energy benefit rate from the perspective of energy saving, and its lower value indicates the better energy efficiency of the system. Total node voltage deviation measures the system from the perspective of power quality, and the lower its value indicates the smoother the system voltage fluctuation and the better the power quality. Total economic cost evaluates the system from the perspective of economic efficiency, and the lower its value indicates that the system is more economically efficient.

Comparative experiments are carried out in four scenarios to verify the effectiveness of the proposed model in IEEE 33 system. The four scenarios are set up as follows.

Case1: Without considering DGs, network reconfiguration and reactive power optimization, ADN operates normally.

Case2: Considering PV and WT, ADN only performs dynamic reconfiguration.

Case3: Considering PV and WT, ADN only performs reactive power optimization.

Case4: Considering PV and WT, using the proposed model, ADN performs dynamic reconfiguration and reactive power coordination optimization.

Table 15. 24-hour simulation results of three scenarios in the IEEE 33 system

Time	Open Switches			$\{Q_{SVC}(kVar)\}^{node}$			$\{N_{sc}\}^{node}$		
	Case2	Case3	Case4	Case2	Case3	Case4	Case2	Case3	Case4
1	[7,14,35,32,28]	[33,34,35,36,37]	[7,14,9,32,28]	$\{0\}^{7}$	$\{10\}^{7}$	$\{60\}^{7}$	$\{0\}^{21}$ $\{0\}^{30}$	$\{0\}^{21}$ $\{16\}^{30}$	$\{4\}^{21}$ $\{11\}^{30}$
2	[7,10,35,32,28]	[33,34,35,36,37]	[7,10,35,32,28]	$\{0\}^{7}$	$\{40\}^{7}$	$\{40\}^{7}$	$\{0\}^{21}$ $\{0\}^{30}$	$\{0\}^{21}$ $\{16\}^{30}$	$\{5\}^{21}$ $\{13\}^{30}$
3	[7,10,35,32,28]	[33,34,35,36,37]	[7,14,9,32,28]	$\{0\}^{7}$	$\{0\}^{7}$	$\{60\}^{7}$	$\{0\}^{21}$ $\{0\}^{30}$	$\{0\}^{21}$ $\{16\}^{30}$	$\{2\}^{21}$ $\{10\}^{30}$
4	[7,14,35,32,28]	[33,34,35,36,37]	[7,11,35,32,28]	$\{0\}^{7}$	$\{20\}^{7}$	$\{90\}^{7}$	$\{0\}^{21}$ $\{0\}^{30}$	$\{0\}^{21}$ $\{15\}^{30}$	$\{4\}^{21}$ $\{8\}^{30}$
5	[7,14,35,32,28]	[33,34,35,36,37]	[7,11,35,32,28]	$\{0\}^{7}$	$\{20\}^{7}$	$\{140\}^{7}$	$\{0\}^{21}$ $\{0\}^{30}$	$\{0\}^{21}$ $\{17\}^{30}$	$\{7\}^{21}$ $\{13\}^{30}$
6	[7,14,35,32,28]	[33,34,35,36,37]	[7,11,35,32,28]	$\{0\}^{7}$	$\{0\}^{7}$	$\{90\}^{7}$	$\{0\}^{21}$ $\{0\}^{30}$	$\{0\}^{21}$ $\{18\}^{30}$	$\{5\}^{21}$ $\{10\}^{30}$
7	[7,14,35,32,28]	[33,34,35,36,37]	[7,10,35,32,28]	$\{0\}^{7}$	$\{20\}^{7}$	$\{120\}^{7}$	$\{0\}^{21}$ $\{0\}^{30}$	$\{0\}^{21}$ $\{17\}^{30}$	$\{9\}^{21}$ $\{13\}^{30}$
8	[7,14,35,32,28]	[33,34,35,36,37]	[7,14,9,32,28]	$\{0\}^{7}$	$\{40\}^{7}$	$\{30\}^{7}$	$\{0\}^{21}$ $\{0\}^{30}$	$\{0\}^{21}$ $\{17\}^{30}$	$\{11\}^{21}$ $\{11\}^{30}$

9	[7,14,35,32,28]	[33,34,35,36,37]	[7,14,35,32,28]	{0}^{7}	{230}^{7}	{150}^{7}	{0}^{21} {0}^{30}	{0}^{21} {19}^{30}	{7}^{21} {11}^{30}
10	[7,11,21,32,28]	[33,34,35,36,37]	[4,14,9,32,27]	{0}^{7}	{140}^{7}	{210}^{7}	{0}^{21} {0}^{30}	{0}^{21} {20}^{30}	{1}^{21} {13}^{30}
11	[7,11,21,32,28]	[33,34,35,36,37]	[4,13,9,32,27]	{0}^{7}	{130}^{7}	{200}^{7}	{0}^{21} {0}^{30}	{0}^{21} {20}^{30}	{1}^{21} {16}^{30}
12	[7,11,35,32,28]	[33,34,35,36,37]	[4,12,9,32,28]	{0}^{7}	{160}^{7}	{230}^{7}	{0}^{21} {0}^{30}	{0}^{21} {20}^{30}	{2}^{21} {18}^{30}
13	[7,10,35,32,28]	[33,34,35,36,37]	[4,13,9,32,27]	{0}^{7}	{200}^{7}	{10}^{7}	{0}^{21} {0}^{30}	{0}^{21} {20}^{30}	{0}^{21} {18}^{30}
14	[7,14,35,32,28]	[33,34,35,36,37]	[6,14,9,31,28]	{0}^{7}	{60}^{7}	{530}^{7}	{0}^{21} {0}^{30}	{0}^{21} {20}^{30}	{7}^{21} {12}^{30}
15	[7,14,21,32,28]	[33,34,35,36,37]	[4,34,35,31,28]	{0}^{7}	{30}^{7}	{310}^{7}	{0}^{21} {0}^{30}	{0}^{21} {19}^{30}	{1}^{21} {12}^{30}
16	[7,14,21,32,28]	[33,34,35,36,37]	[7,14,21,32,28]	{0}^{7}	{0}^{7}	{10}^{7}	{0}^{21} {0}^{30}	{0}^{21} {20}^{30}	{2}^{21} {13}^{30}
17	[7,14,35,32,28]	[33,34,35,36,37]	[7,14,35,32,28]	{0}^{7}	{210}^{7}	{250}^{7}	{0}^{21} {0}^{30}	{0}^{21} {20}^{30}	{8}^{21} {15}^{30}
18	[7,10,35,32,28]	[33,34,35,36,37]	[7,14,9,32,28]	{0}^{7}	{10}^{7}	{140}^{7}	{0}^{21} {0}^{30}	{0}^{21} {18}^{30}	{7}^{21} {14}^{30}
19	[7,14,9,32,28]	[33,34,35,36,37]	[7,14,9,32,28]	{0}^{7}	{0}^{7}	{60}^{7}	{0}^{21} {0}^{30}	{0}^{21} {20}^{30}	{10}^{21} {17}^{30}
20	[7,14,9,32,28]	[33,34,35,36,37]	[7,14,9,32,28]	{0}^{7}	{10}^{7}	{80}^{7}	{0}^{21} {0}^{30}	{0}^{21} {20}^{30}	{10}^{21} {13}^{30}
21	[7,14,9,32,28]	[33,34,35,36,37]	[7,14,9,32,28]	{0}^{7}	{20}^{7}	{140}^{7}	{0}^{21} {0}^{30}	{0}^{21} {20}^{30}	{8}^{21} {14}^{30}
22	[7,14,9,32,28]	[33,34,35,36,37]	[7,14,9,32,28]	{0}^{7}	{30}^{7}	{10}^{7}	{0}^{21} {0}^{30}	{0}^{21} {18}^{30}	{9}^{21} {13}^{30}
23	[7,14,9,32,28]	[33,34,35,36,37]	[7,14,9,32,28]	{0}^{7}	{0}^{7}	{60}^{7}	{0}^{21} {0}^{30}	{0}^{21} {18}^{30}	{14}^{21} {14}^{30}
24	[7,10,35,32,28]	[33,34,35,36,37]	[7,14,9,32,28]	{0}^{7}	{0}^{7}	{60}^{7}	{0}^{21} {0}^{30}	{0}^{21} {17}^{30}	{5}^{21} {9}^{30}

Table 16. The 24-hour total loss, total voltage deviation and total economic cost in four scenarios in the IEEE 33 system

Case	Total power loss (kW)	Total voltage deviation (p.u)	Total economic cost ($)
Case1	3.2685E+03	1.9776	4.4620E+04
Case2	1.0802E+03	0.8196	**2.4837E+04**
Case3	1.2210E+03	0.8820	4.5591E+04
Case4	**7.9216E+02**	**0.5920**	5.0910E+04

Case1 is the basic case and has not been optimized. Table 15 shows the 24-hour optimization results for Case2 to Case4. Table 16 shows the 24-hour goal values under four

scenarios in IEEE 33 system. The bold font is the optimal value of each goal. In the Case2, compared with the initial state Case1, the total network loss, total voltage deviation and total economic cost are reduced by 66.95%, 58.56% and 44.34%. In the Case3, compared with the initial state Case1, the network loss is reduced by 62.64% and the voltage deviation is reduced by 58.56%. Case3 uses reactive power compensation device for compensation, considering the cost of the device, so the total economic cost increases by 2.18%. In the Case4, the total network loss and total voltage deviation are reduced by 75.76% and 70.06% compared with the initial state Case1. Case4 performs reactive power compensation and dynamic reconfiguration, considering the cost of devices and the switching cost of the contact switch, so the total economic cost increases by 14.10%, and the other two goals are significantly reduced. In the Case4, the lowest values are achieved on the total power loss and total voltage deviation. Compared with Case2, the total power loss and total voltage deviation in Case4 are reduced by 22.67% and 27.77%.

The total power loss and total voltage deviation in Case4 are reduced by 35.12% and 32.88% compared with Case3. Case4 also considers the switching cost of dynamic reconfiguration, so the total economic cost is higher than Case3, but the other two indicators are significantly better than Case3. Case3 only performs reactive power optimization. Although the total economic cost is saved, the values of other indicators are higher than Case4 and the power quality is lower than Case4. Considering PV and WT, real-time electricity prices and time-varying load conditions, the proposed model is used for dynamic reconfiguration and reactive power coordination optimization of ADN, which significantly reduces the active power loss, voltage deviation and energy loss and effectively improves power quality.

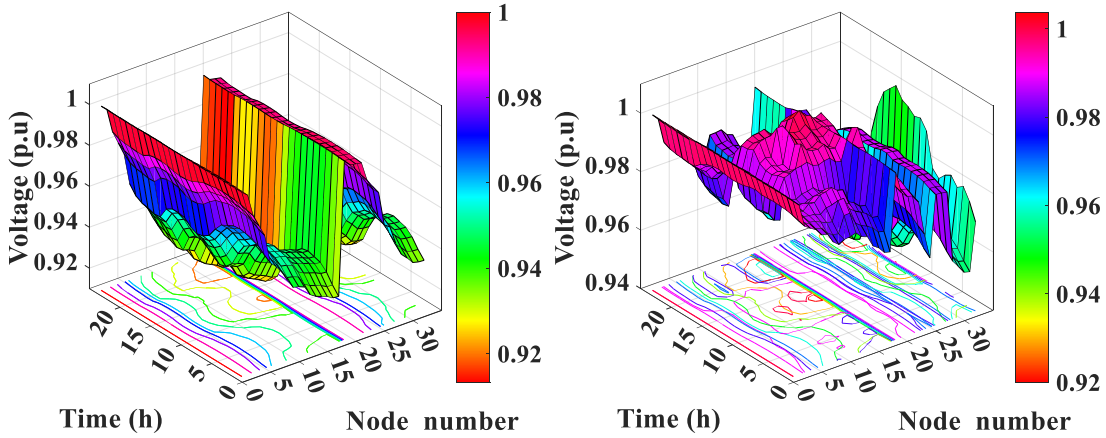

(a) Voltage distribution of case 1

(b) Voltage distribution of case 2

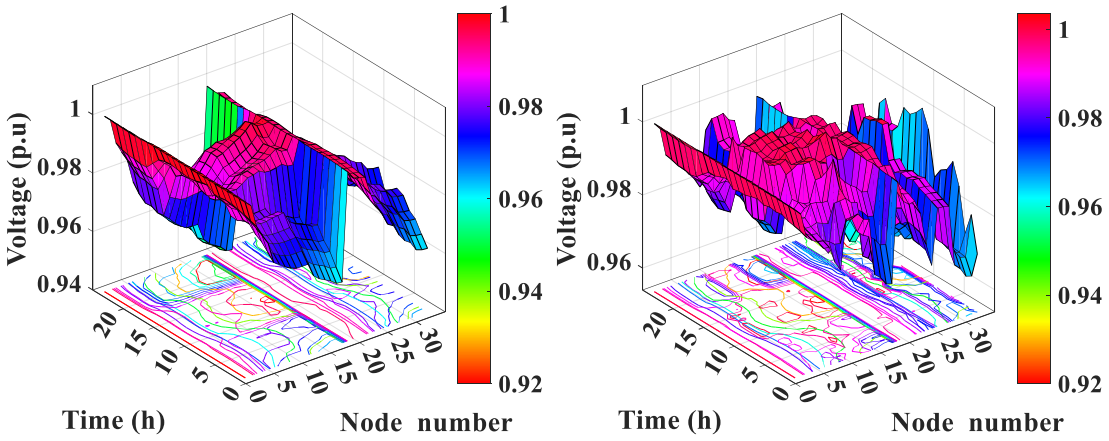

(c) Voltage distribution of case 3 (d) Voltage distribution of case 4

Figure 8. Three-dimensional diagram of the 24-hour node voltage distribution under four cases

Figure 8 shows a 3-dimensional graph of the 24-hour node voltage distribution under four scenarios. Case1 does not perform network reconfiguration and reactive power optimization. The minimum value of the node voltage within 24-hour fluctuates around 0.93 and the node voltage fluctuates greatly. Most of the node voltages are concentrated around 0.94. The node voltage is too low and the power quality is poor. Case2 only performs dynamic reconfiguration. The minimum value of the node voltage within 24-hour is around 0.95, and a large number of node voltage values are concentrated around 0.97.

Case3 only performs reactive power optimization. The lowest voltage mainly fluctuates around 0.96 and most of the voltage is concentrated around 0.98. Compared with Case1, the voltage fluctuations of the Case2 and Case3 are weakened and the power quality is improved. DG access, network reconfiguration and reactive power optimization can reduce voltage fluctuation, but there is still much room for improvement. Case4 uses the proposed model to carry out ADN integrated optimization. The minimum node voltage fluctuates around 0.97 and the number is small. Most of the voltage values are concentrated around 0.99. The node voltage fluctuations are significantly smaller than those in Case1, Case2 and Case3, effectively smoothing the network voltage fluctuations and the power quality is significantly improved.

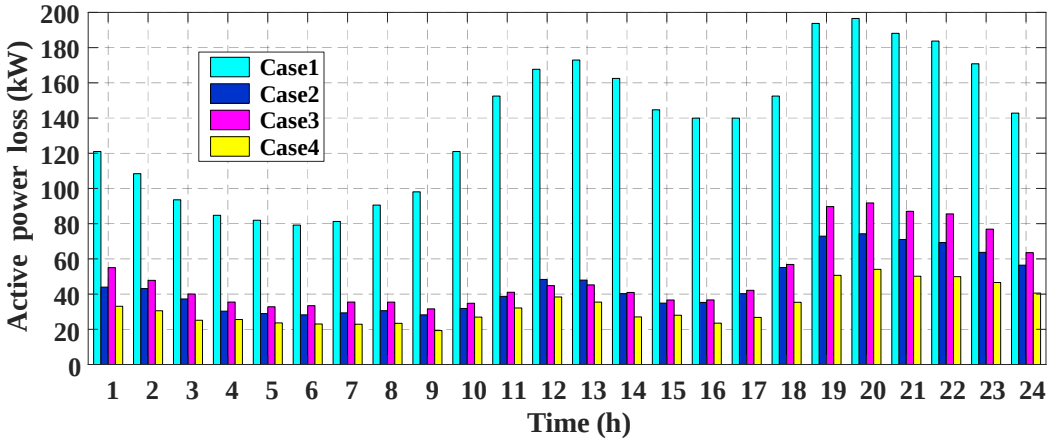

Figure 9. 24-hour active power loss under four scenarios

Figure 9 shows the 24-hour power loss in four scenarios. Case2 and Case3 have a

decrease in network loss every hour compared with the initial state Case1. Dynamic reconfiguration, reactive power optimization and DG access can all reduce network losses, but there is still much room for improvement. Case4 has the least power loss every hour. The proposed model can effectively optimize the operation of ADN, reduce power loss and energy waste compared with Case1, Case2 and Case3.

5. Concluding Remarks

This study uses a new MOSSA-based optimization method to solve the ADN integrated optimization problem considering distributed power sources, real-time tariffs and time-varying loads. The ADN optimization problem is a multi-dimensional and multi-constrained nonlinear optimization problem. Hence, this study proposes MOSSA to solve ADN integrated optimization problem considering photovoltaic, wind power and dynamic load, and the effectiveness is verified. In addition, the ADN integrated optimization mathematical model is constructed based on the goals of minimizing power loss, economic cost and node voltage deviation, and multiple scenarios are established in classical test system to verify the validity of the proposed method. The following are the findings of this study.

- The MOSSA is tested by ZDT series test functions, and its convergence, solution set distribution and comprehensive performance are proved to outperform NSMFO, NSGA-II, MOPSO and MOGWO.
- The ADN integrated optimization model considering photovoltaic, wind power, dynamic load and real-time tariff is constructed, and the MOSSA-based approach formulates an excellent optimization scheme with the highest power quality and the best energy and economic benefits.
- The lowest total power loss and total node voltage obtained by the proposed MOSSA in the IEEE 33 test system are 792.16KW and 0.592 p.u, with most of the voltage values concentrated on 0.99 p.u. Compared to the initial state, the total power loss and total node voltage deviation obtained by MOSSA are reduced by 75.76% and 70.06%.

This study is significance to the realization of sustainable energy. The proposed MOSSA has better optimization performance and can be regarded as an effective means to solve the ADN dynamic reconfiguration integrated optimization problem. The proposed dynamic reconfiguration integrated optimization model of ADN provides an effective solution to reduce energy loss and improve power quality of ADN. However, this study has limitations because the randomness of photovoltaic power generation and wind power generation is not considered. More factors should be considered in future studies to make the research results more suitable for actual projects. In addition, more forms of renewable energy can be added to the system for increasing the penetration rate of renewable energy, and achieving the goals of carbon peak and carbon neutral.

Acknowledgements

This work was supported by the key project of Tianjin Natural Science Foundation [Project No. 19JCZDJC32100] and the Natural Science Foundation of Hebei Province of China

[Project No. E2018202282].

References

1. Acharya, S., Ganesan, S., Kumar, D. V., & Subramanian, S. (2021). A multi-objective multi-verse optimization algorithm for dynamic load dispatch problems. *Knowledge-Based Systems, 231*.
2. Azad-Farsani, E., Sardou, I. G., & Abedini, S. (2021). Distribution Network Reconfiguration based on LMP at DG connected busses using game theory and self-adaptive FWA. *Energy, 215*, 119146.
3. Azizivahed, A., Narimani, H., Fathi, M., Naderi, E., Safarpour, H. R., & Narimani, M. R. (2018). Multi-objective dynamic distribution feeder reconfiguration in automated distribution systems. *Energy, 147*, 896-914.
4. Azizivahed, A., Narimani, H., Naderi, E., Fathi, M., & Narimani, M. R. (2017). A hybrid evolutionary algorithm for secure multi-objective distribution feeder reconfiguration. *Energy, 138*, 355-373.
5. Carrasco, J., Garcia, S., Rueda, M. M., Das, S., & Herrera, F. (2020). Recent trends in the use of statistical tests for comparing swarm and evolutionary computing algorithms: Practical guidelines and a critical review. *Swarm and Evolutionary Computation, 54*.
6. Chen, J., Zhang, F., & Zhang, Y. (2011). Distribution Network Reconfiguration Based on Simulated Annealing Immune Algorithm. *Energy Procedia, 12*, 271-277.
7. Chen, S., Li, P., Ji, H., Yu, H., Yan, J., Wu, J., & Wang, C. (2021). Operational flexibility of active distribution networks with the potential from data centers. *Applied Energy, 293*, 116935.
8. Chen, X., & Tang, G. W. (2022). Solving static and dynamic multi-area economic dispatch problems using an improved competitive swarm optimization algorithm. *Energy, 238*.
9. Cheng, S., & Li, Z. (2019). Multi-objective Network Reconfiguration Considering V2G of Electric Vehicles in Distribution System with Renewable Energy. *Energy Procedia, 158*, 278-283.
10. Chittur Ramaswamy, P., Tant, J., Pillai, J. R., & Deconinck, G. (2015). Novel methodology for optimal reconfiguration of distribution networks with distributed energy resources. *Electric Power Systems Research, 127*, 165-176.
11. Coelho, L. D., & Mariani, V. C. (2006). Particle swarm optimization with quasi-newton local search for solving economic dispatch problem. *2006 IEEE International Conference on Systems, Man, and Cybernetics, Vols 1-6, Proceedings*, 3109.
12. Coelho, L. D., & Mariani, V. C. (2007). Economic dispatch optimization using hybrid chaotic particle swarm optimizer. *2007 IEEE International Conference on Systems, Man and Cybernetics, Vols 1-8*, 3428.
13. Coelho, L. D., & Mariani, V. C. (2009). Chaotic artificial immune approach applied to economic dispatch of electric energy using thermal units. *Chaos Solitons & Fractals, 40*(5), 2376-2383.
14. Coelho, L. D., Mariani, V. C., Guerra, F. A., da Luz, M. V. F., & Leite, J. V. (2014). Multiobjective Optimization of Transformer Design Using a Chaotic Evolutionary Approach. *IEEE Transactions on Magnetics, 50*(2).
15. Coello Coello, C. A. (2002). Theoretical and numerical constraint-handling techniques used with evolutionary algorithms: a survey of the state of the art. *Computer Methods in Applied Mechanics and Engineering, 191*(11), 1245-1287.
16. Derrac, J., Garcia, S., Hui, S., Suganthan, P. N., & Herrera, F. (2014). Analyzing convergence performance of evolutionary algorithms: A statistical approach. *Information Sciences, 289*,

41-58.

17. Duan, D.-L., Ling, X.-D., Wu, X.-Y., & Zhong, B. (2015). Reconfiguration of distribution network for loss reduction and reliability improvement based on an enhanced genetic algorithm. *International Journal of Electrical Power & Energy Systems, 64*, 88-95.
18. Gao, J., Gao, F., Ma, Z., Huang, N., & Yang, Y. (2021). Multi-objective optimization of smart community integrated energy considering the utility of decision makers based on the Lévy flight improved chicken swarm algorithm. *Sustainable Cities and Society, 72*, 103075.
19. Guimarães, I. G., Bernardon, D. P., Garcia, V. J., Schmitz, M., & Pfitscher, L. L. (2021). A decomposition heuristic algorithm for dynamic reconfiguration after contingency situations in distribution systems considering island operations. *Electric Power Systems Research, 192*, 106969.
20. Gupta, N., Swarnkar, A., & Niazi, K. R. (2014). Distribution network reconfiguration for power quality and reliability improvement using Genetic Algorithms. *International Journal of Electrical Power & Energy Systems, 54*, 664-671.
21. Jafari, A., Ganjeh Ganjehlou, H., Baghal Darbandi, F., Mohammadi-Ivatloo, B., & Abapour, M. (2020). Dynamic and multi-objective reconfiguration of distribution network using a novel hybrid algorithm with parallel processing capability. *Applied Soft Computing, 90*, 106146.
22. Ji, X., Yin, Z., Zhang, Y., Xu, B., & liu, Q. (2021). Real-time autonomous dynamic reconfiguration based on deep learning algorithm for distribution network. *Electric Power Systems Research, 195*, 107132.
23. Jiang, S., & Yang, S. (2016). An Improved Multiobjective Optimization Evolutionary Algorithm Based on Decomposition for Complex Pareto Fronts. *IEEE Transactions on Cybernetics, 46*(2), 421-437.
24. Kefayat, M., Lashkar Ara, A., & Nabavi Niaki, S. A. (2015). A hybrid of ant colony optimization and artificial bee colony algorithm for probabilistic optimal placement and sizing of distributed energy resources. *Energy Conversion and Management, 92*, 149-161.
25. Kiani, H., Hesami, K., Azarhooshang, A., Pirouzi, S., & Safaee, S. (2021). Adaptive robust operation of the active distribution network including renewable and flexible sources. *Sustainable Energy, Grids and Networks, 26*, 100476.
26. Kovački, N. V., Vidović, P. M., & Sarić, A. T. (2018). Scalable algorithm for the dynamic reconfiguration of the distribution network using the Lagrange relaxation approach. *International Journal of Electrical Power & Energy Systems, 94*, 188-202.
27. Li, L. L., Liu, Z. F., Tseng, M. L., Zheng, S. J., & Lim, M. K. (2021). Improved tunicate swarm algorithm: Solving the dynamic economic emission dispatch problems. *Applied Soft Computing, 108*.
28. Li, M., Yang, S., & Liu, X. (2016). Pareto or Non-Pareto: Bi-Criterion Evolution in Multiobjective Optimization. *IEEE Transactions on Evolutionary Computation, 20*(5), 645-665.
29. Liu, Z. F., Li, L. L., Liu, Y. W., Liu, J. Q., Li, H. Y., & Shen, Q. (2021). Dynamic economic emission dispatch considering renewable energy generation: A novel multi-objective optimization approach. *Energy, 235*.
30. Ma, W., Wang, W., Chen, Z., Wu, X., Hu, R., Tang, F., & Zhang, W. (2021). Voltage regulation methods for active distribution networks considering the reactive power optimization of substations. *Applied Energy, 284*, 116347.
31. Mahdad, B. (2019). Optimal reconfiguration and reactive power planning based fractal search

algorithm: A case study of the Algerian distribution electrical system. *Engineering Science and Technology, an International Journal, 22*(1), 78-101.

32. Medani, K. b. o., Sayah, S., & Bekrar, A. (2018). Whale optimization algorithm based optimal reactive power dispatch: A case study of the Algerian power system. *Electric Power Systems Research, 163*, 696-705.
33. Mellal, M. A., & Williams, E. J. (2020). Cuckoo optimization algorithm with penalty function and binary approach for combined heat and power economic dispatch problem. *Energy Reports, 6*, 2720-2723.
34. Mirjalili, S., Jangir, P., Mirjalili, S. Z., Saremi, S., & Trivedi, I. N. (2017). Optimization of problems with multiple objectives using the multi-verse optimization algorithm. *Knowledge-Based Systems, 134*, 50-71.
35. Mirjalili, S., Saremi, S., Mirjalili, S. M., & Coelho, L. d. S. (2016). Multi-objective grey wolf optimizer: A novel algorithm for multi-criterion optimization. *Expert Systems with Applications, 47*, 106-119.
36. Mukhopadhyay, B., & Das, D. (2020). Multi-objective dynamic and static reconfiguration with optimized allocation of PV-DG and battery energy storage system. *Renewable and Sustainable Energy Reviews, 124*, 109777.
37. Nguyen, T. T., & Nguyen, T. T. (2019). An improved cuckoo search algorithm for the problem of electric distribution network reconfiguration. *Applied Soft Computing, 84*, 105720.
38. Nguyen, T. T., Nguyen, T. T., Nguyen, N. A., & Duong, T. L. (2021). A novel method based on coyote algorithm for simultaneous network reconfiguration and distribution generation placement. *Ain Shams Engineering Journal, 12*(1), 665-676.
39. Nguyen, T. T., & Truong, A. V. (2015). Distribution network reconfiguration for power loss minimization and voltage profile improvement using cuckoo search algorithm. *International Journal of Electrical Power & Energy Systems, 68*, 233-242.
40. Nick, M., Cherkaoui, R., & Paolone, M. (2014). Optimal Allocation of Dispersed Energy Storage Systems in Active Distribution Networks for Energy Balance and Grid Support. *IEEE Transactions on Power Systems, 29*(5), 2300-2310.
41. Niknam, T., Fard, A. K., & Seifi, A. (2012). Distribution feeder reconfiguration considering fuel cell/wind/photovoltaic power plants. *Renewable Energy, 37*(1), 213-225.
42. Oh, S. H., Yoon, Y. T., & Kim, S. W. (2020). Online reconfiguration scheme of self-sufficient distribution network based on a reinforcement learning approach. *Applied Energy, 280*, 115900.
43. Olamaei, J., Niknam, T., & Gharehpetian, G. (2008). Application of particle swarm optimization for distribution feeder reconfiguration considering distributed generators. *Applied Mathematics and Computation, 201*(1), 575-586.
44. Pathan, M. I., Al-Muhaini, M., & Djokic, S. Z. (2020). Optimal reconfiguration and supply restoration of distribution networks with hybrid microgrids. *Electric Power Systems Research, 187*, 106458.
45. Qian, W. Y., & Sui, A. D. (2021). A novel structural adaptive discrete grey prediction model and its application in forecasting renewable energy generation. *Expert Systems with Applications, 186*.
46. Raposo, A. A. M., Rodrigues, A. B., & da Guia da Silva, M. (2020). Robust meter placement for state estimation considering Distribution Network Reconfiguration for annual energy loss reduction. *Electric Power Systems Research, 182*, 106233.
47. Raut, U., & Mishra, S. (2019). An improved Elitist–Jaya algorithm for simultaneous network

reconfiguration and DG allocation in power distribution systems. *Renewable Energy Focus, 30*, 92-106.

48. Ru-tian, W., Yan-liang, Y., Bin, W., Xing-wei, W., Jin-wei, H., & Shu-zhen, Z. (2012). Application of Optimization Algorithm on Simulating the Fisher Fishing in Multi-objective Optimal Reactive Power. *Energy Procedia, 17*, 1482-1489.
49. Sapre, S., & S, M. (2021). Emulous mechanism based multi-objective moth–flame optimization algorithm. *Journal of Parallel and Distributed Computing, 150*, 15-33.
50. Shariatkhah, M.-H., Haghifam, M.-R., Salehi, J., & Moser, A. (2012). Duration based reconfiguration of electric distribution networks using dynamic programming and harmony search algorithm. *International Journal of Electrical Power & Energy Systems, 41*(1), 1-10.
51. Sheidaei, F., Ahmarinejad, A., Tabrizian, M., & Babaei, M. (2021). A stochastic multi-objective optimization framework for distribution feeder reconfiguration in the presence of renewable energy sources and energy storages. *Journal of Energy Storage, 40*, 102775.
52. Singh, P., Meena, N. K., Yang, J., Vega-Fuentes, E., & Bishnoi, S. K. (2020). Multi-criteria decision making monarch butterfly optimization for optimal distributed energy resources mix in distribution networks. *Applied Energy, 278*, 115723.
53. Srinivasan, G. (2021). Optimization of distributed generation units in reactive power compensated reconfigured distribution network. *Automatika, 62*(2), 249-263.
54. Su, C.-T., Chang, C.-F., & Chiou, J.-P. (2005). Distribution network reconfiguration for loss reduction by ant colony search algorithm. *Electric Power Systems Research, 75*(2), 190-199.
55. Sun, W. Z., Zhang, H., Tseng, M.-L., Weipeng, Z., & Xinyang, L. (2021). Hierarchical energy optimization management of active distribution network with multi-microgrid system. *Journal of Industrial and Production Engineering*, 1-20.
56. Tavana, M., Li, Z., Mobin, M., Komaki, M., & Teymourian, E. (2016). Multi-objective control chart design optimization using NSGA-III and MOPSO enhanced with DEA and TOPSIS. *Expert Systems with Applications, 50*, 17-39.
57. Tolabi, H. B., Ara, A. L., & Hosseini, R. (2020). A new thief and police algorithm and its application in simultaneous reconfiguration with optimal allocation of capacitor and distributed generation units. *Energy, 203*, 117911.
58. Tran, T. T., Truong, K. H., & Vo, D. N. (2020). Stochastic fractal search algorithm for reconfiguration of distribution networks with distributed generations. *Ain Shams Engineering Journal, 11*(2), 389-407.
59. Tseng, ML., Tran, TPT., Ha, H.M., Bui, TD., & Lim, M.K. (2021). Sustainable industrial and operation engineering trends and challenges Toward Industry 4.0: a data driven analysis. *Journal of Industrial and Production Engineering*, 38:8, 581-598, DOI: 10.1080/21681015.2021.1950227
60. Wang, X. H., & Zhang, Y. M. (2011). Multi-Objective Reactive Power Optimization Based On The Fuzzy Adaptive Particle Swarm Algorithm. *Procedia Engineering, 16*, 230-238.
61. Xu, T., Ren, Y., Guo, L., Wang, X., Liang, L., & Wu, Y. (2021). Multi-objective robust optimization of active distribution networks considering uncertainties of photovoltaic. *International Journal of Electrical Power & Energy Systems, 133*, 107197.
62. Xue, J., & Shen, B. (2020). A novel swarm intelligence optimization approach: sparrow search algorithm. *Systems Science & Control Engineering, 8*(1), 22-34.

63. Zhang, P., Qian, Y., & Qian, Q. (2021). Multi-objective optimization for materials design with improved NSGA-II. *Materials Today Communications, 28*, 102709.
64. Zidan, A., & El-Saadany, E. F. (2013). Distribution system reconfiguration for energy loss reduction considering the variability of load and local renewable generation. *Energy, 59*, 698-707.
65. Zou, L. (2021). Design of reactive power optimization control for electromechanical system based on fuzzy particle swarm optimization algorithm. *Microprocessors and Microsystems, 82*, 103865.